Plasmamembrane-localization of apoptotic caspases for non-apoptotic functions

Amcheslavsky, Alla; Wang, Shiuan; Fogarty, Caitlin; Lindblad, Jillian; Fan, Yun; Bergmann, Andreas

DOI:
10.1016/j.devcel.2018.04.020

Document Version
Peer reviewed version

Citation for published version (Harvard):
Amcheslavsky, A, Wang, S, Fogarty, C, Lindblad, J, Fan, Y & Bergmann, A 2018, 'Plasmamembrane-localization of apoptotic caspases for non-apoptotic functions' Developmental Cell, vol. 45, no. 4, pp. 450-464.e3. https://doi.org/10.1016/j.devcel.2018.04.020

Plasmamembrane-localization of apoptotic caspases for non-apoptotic functions

Running title: Myo1D translocates Dronc to the plasmamembrane

Alla Amcheslavsky[1], Shiuan Wang[2], Caitlin E. Fogarty[1], Jillian L. Lindblad[1], Yun Fan[3] and Andreas Bergmann[1,*]

[1] University of Massachusetts Medical School
Department of Molecular, Cell and Cancer Biology
364 Plantation Street
Worcester, MA 01605
USA

[2] Program in Developmental Biology
Baylor College of Medicine
Houston, TX 77030
USA

[3] University of Birmingham
School of Biosciences
Edgbaston
Birmingham B15 2TT
UK

* Lead contact (corresponding author): Andreas.Bergmann@umassmed.edu
Tel. +1 518.856.6234
Fax +1 518.856.1310

Summary

Caspases are best characterized for their function in apoptosis. However, they also have non-apoptotic functions such as apoptosis-induced proliferation (AiP) where caspases release mitogens for compensatory proliferation independently of their apoptotic role. Here, we report that the unconventional myosin, Myo1D, which is known for its involvement in left/right development, is an important mediator of AiP in *Drosophila*. Mechanistically, Myo1D translocates the initiator caspase Dronc to the basal side of the plasmamembrane of epithelial cells where Dronc promotes the activation of the NADPH-oxidase Duox for ROS generation and AiP in a non-apoptotic manner. We propose that the basal side of the plasmamembrane constitutes a non-apoptotic compartment for caspases. Finally, Myo1D promotes tumor growth and invasiveness of the neoplastic *scrib* Ras^{V12} model. Together, we identified a novel function of Myo1D for AiP and tumorigenesis, and reveal a mechanism by which cells sequester apoptotic caspases in a non-apoptotic compartment at the plasmamembrane.

Keywords: Apoptosis-induced proliferation, *Drosophila*, Dronc, Myo1D, non-apoptotic functions, plasmamembrane

Introduction

Under stress conditions when a large number of cells are dying, there is a need for compensatory proliferation to replace the lost cells with new cells. Work using several model organisms has shown that under these conditions, apoptotic cells can release mitogenic signals that induce proliferation of surviving cells for the replacement of dying cells (Chera et al., 2009; Huh et al., 2004; Li et al., 2010; Perez-Garijo et al., 2004; Ryoo et al., 2004; Tseng et al., 2007). Because apoptotic cells are actively triggering this type of compensatory proliferation, this process has been termed apoptosis-induced proliferation (AiP) (Mollereau et al., 2013).

Caspases are Cys proteases that are the main effectors of apoptosis (reviewed by (Salvesen et al., 2016; Shalini et al., 2015)). They are produced as inactive zymogens with a prodomain and after processing a large and small subunit. There are initiator and effector caspases. Initiator caspases carry protein/protein interacting motifs in their prodomains which mediate their incorporation into large multimeric protein complexes. For example, the mammalian initiator Caspase-9 is recruited into the Apaf-1 apoptosome, while its *Drosophila* ortholog Dronc forms the apoptosome with the Apaf-1 homolog Dark (reviewed by (Yuan and Akey, 2013)). Effector caspases such as mammalian Caspase-3 or *Drosophila* DrICE and Dcp-1 are proteolytically processed by activated initiator caspases and mediate the apoptotic process.

In addition to apoptosis, caspases are also mediating AiP. They trigger the release of Wnt, BMP/TGF-β, EGF and Hh mitogens for AiP (Chera et al., 2009; Fan and Bergmann, 2008a, b, 2014; Huh et al., 2004; Li et al., 2010; Perez-Garijo et al., 2004; Ryoo et al., 2004). This has been best studied for the *Drosophila* initiator caspase Dronc using the "undead" AiP model in which apoptotic signaling is induced by expression of upstream cell death factors such as *hid*, but the execution of apoptosis is blocked by co-expression of the effector caspase

inhibitor *p35*, thus rendering cells in an "undead" condition (Martin et al., 2009). Because P35 inhibits apoptosis, but not Dronc, Dronc can still mediate non-apoptotic functions such as AiP. When *hid* and *p35* are co-expressed using the *ey-Gal4* driver (*ey>hid,p35*) which is expressed in epithelial cells of eye imaginal discs, Dronc continuously signals for AiP and triggers hyper-proliferation. Consequently, the discs are enlarged and the resulting heads of the adult flies are overgrown (the phenotypic classes of *ey>hid,p35*-induced overgrowth are shown in Figure S1A-D). In genetic screens, we are screening for suppressors of the overgrowth phenotype of undead (*ey>hid,p35*) adult heads to identify genes and mechanisms involved in AiP (Fan et al., 2014).

Mechanistically, we showed that in undead cells, Dronc stimulates the NADPH-oxidase Duox for the production of extracellular reactive oxygen species (eROS) (Fogarty et al., 2016). eROS recruit and activate hemocytes, *Drosophila* immune cells similar to macrophages, to the undead imaginal disc. In turn, hemocytes release the TNF-like ligand Eiger which induces JNK activity in epithelial disc cells. JNK promotes the expression of the apoptotic genes *reaper* and *hid* which initiate a positive feedback loop to maintain undead signaling (Fogarty et al., 2016). In addition, it induces the release of the mitogens Wingless (Wg), a Wnt-like gene in *Drosophila*, Decapentaplegic (Dpp), a BMP/TGF-β homolog and Spitz (Spi), an EGF ligand (Fan et al., 2014; Huh et al., 2004; Perez-Garijo et al., 2004; Ryoo et al., 2004) which all promote AiP.

In addition to undead AiP, there is also "genuine" AiP during which dying cells complete the apoptotic process and the response of the affected tissue to replace the dying cells is examined (Fan and Bergmann, 2008b; Fan et al., 2014; Herrera et al., 2013; Santabarbara-Ruiz et al., 2015; Smith-Bolton et al., 2009). In contrast to undead AiP, genuine AiP does not promote overgrowth. Therefore, although most genes identified in undead AiP also have important roles in genuine AiP, there must be differences between the two AiP models. In any case, genuine AiP

is used as a model of tissue regeneration, while the hyper-proliferation of undead AiP serves as a tumorigenic model (reviewed in (Fogarty and Bergmann, 2015, 2017)).

Class I unconventional myosins are conserved actin-based motor proteins, composed of the N-terminal head (motor) region with an ATP-binding motif (including P-, switch1- and switch2-loops) and an actin-binding domain, a neck region characterized by two to three IQ motifs and a C-terminal tail domain that interacts with phospholipids at membranes (Figure 2A) (reviewed in (Barylko et al., 2000; Coluccio, 1997)). Mammals have eight class I myosins, *Drosophila* has three, *Myosin 1D* (*Myo1D,* aka *Myo31DF*), *MyoIC* (*Myo61F*) and *Myo95E* (Morgan et al., 1995; Morgan et al., 1994; Okumura et al., 2015; Tzolovsky et al., 2002). While *Myo1D* and *Myo1C* are involved in left/right (L/R) development of visceral organs, the function of *Myo95E* is unknown (Hozumi et al., 2006; Okumura et al., 2015; Speder et al., 2006).

Although *Drosophila* is a bilateral organism, certain visceral organs such as the gut and the coiling of the spermiducts around the gut which occurs in a morphogenetic movement termed male terminalia rotation, display L/R asymmetry (Coutelis et al., 2014; Geminard et al., 2014; Hayashi and Murakami, 2001; Kuranaga et al., 2011; Ligoxygakis et al., 2001; Petzoldt et al., 2012; Speder et al., 2006; Suzanne et al., 2010). In *Myo1D* mutants, the chirality of these asymmetric organs and movements are reversed (Hozumi et al., 2006; Speder et al., 2006). For example, the male terminalia rotation during pupal development which in wild-type occurs for 360° in clockwise (dextral) orientation, proceeds in *Myo1D* mutants sinistrally, defining *Myo1D* as dextral determinant (Hozumi et al., 2006; Speder et al., 2006). Myo1D engages the actin cytoskeleton and adherens junctions for this movement (Petzoldt et al., 2012).

Overexpression of Myo1C antagonizes the dextral activity of Myo1D by displacing it from adherens junctions (Hozumi et al., 2008; Petzoldt et al., 2012). However, the loss-of-

function phenotype of *Myo1C* did not confirm this antagonizing function. Instead, while Myo1C single mutants do not display any L/R defect, the *Myo1C Myo1D* double mutant has a stronger sinistral male terminalia phenotype than *Myo1D* mutants indicating that Myo1C has a partially redundant dextral activity with Myo1D (Okumura et al., 2015).

It has long been known that genes in the apoptosis pathway such as *hid*, *dronc* and *drICE* are also involved in male terminalia rotation in *Drosophila* (Abbott and Lengyel, 1991; Grether et al., 1995; Kamber Kaya et al., 2017; Krieser et al., 2007; Macias et al., 2004; Muro et al., 2006). Indeed, localized apoptotic activity is required for this L/R process (Kuranaga et al., 2011; Suzanne et al., 2010). How Myo1D and the apoptosis pathway interact for male terminalia rotation is not very well understood. Interestingly, mutants of the JNK signaling pathway or overexpression of *puckered*, an inhibitor of JNK activity, also display defects in male terminalia rotation (Glise et al., 1995; Holland et al., 1997; Macias et al., 2004; Rousset et al., 2010).

Here, we report that *Myo1D* is an essential component of AiP in the undead model. Genetic inactivation of *Myo1D* strongly suppresses *ey>hid,p35*-induced overgrowth of the head capsule, while overexpression of *Myo1D* enhances it. Myo1D promotes the generation of ROS by Duox for AiP signaling. Further mechanistic analysis reveals that Myo1D is required for membrane localization of Dronc, specifically to the basal side of the plasmamembrane of undead epithelial disc and salivary gland cells. Here, Dronc exerts a non-apoptotic function resulting in Duox activation. We propose that the basal side of the plasmamembrane constitutes a non-apoptotic compartment which allows non-apoptotic processes of Dronc and potentially other caspases to occur. Therefore, in addition to the dextral activity of Myo1D, we identified a novel function of Myo1D for the control of apoptosis-induced proliferation.

Results

Myo1D is necessary and sufficient for generation of ROS in undead tissue

In a RNAi modifier screen, we identified two independent *Myo1D* RNAi lines as strong suppressors of *ey>hid,p35*-induced head overgrowth (Figure 1A-F). In addition, two *Myo1D* mutant alleles dominantly suppressed *ey>hid,p35*-induced overgrowth (Figure 1A,G,H). Conversely, mis-expression of *Myo1D* strongly enhanced *ey>hid,p35*-induced overgrowth (Figure 1A,I). A control *UAS* line (*UAS-EV*) did not modify AiP-overgrowth (Figure 1A,D).

To determine how *Myo1D* controls AiP, we first considered that it may control AiP indirectly through regulation of apoptosis. However, *Myo1D* RNAi does not significantly change apoptosis in two apoptosis models in the eye (*GMR-hid*) and wing (*nub-hid*) imaginal discs (Figure S1E-I') suggesting that *Myo1D* does not affect cell death, but is directly involved in driving proliferation of AiP.

To identify the step in which Myo1D is involved in the AiP pathway, we tested the dependence of several AiP markers on *Myo1D*. Indeed, *Myo1D* RNAi suppressed ectopic JNK activity and Wg expression in undead tissue (Figure 1J-L'; Figure S1J-K') suggesting that *Myo1D* acts upstream of these markers. Because JNK activity is induced by Eiger signaling in the undead model (Fogarty et al., 2016), we examined if Myo1D is involved in Eiger signaling using the *GMR>Eiger* model. However, *Myo1D* RNAi does not suppress *GMR-Eiger*-induced eye ablation (Figure S2), suggesting that Myo1D is not part of the Eiger signaling pathway.

Recently, we showed that undead AiP involves ROS generation and activation of hemocytes (Fogarty et al., 2016). In control eye/antennal discs, hemocytes form cellular clusters at the antennal disc and along the morphogenetic furrow of the eye disc (Figure 1M,M').

However, at undead eye discs, hemocytes cover large portions of the eye discs, single out from the cellular clusters and extend cytoplasmic protrusions in an ROS-dependent manner (Figure 1N,N',P) (Fogarty et al., 2016). Depletion of *Myo1D* results in the failure of the hemocytes to adopt the activated morphology (Figure 1O,O',P). In addition, reducing *Myo1D* activity causes loss of DHE labeling, a ROS indicator (Figure 1Q-T). These data place Myo1D upstream of ROS generation in the AiP pathway (Figure 1U).

While overexpression of *Myo1D* by *ey-Gal4* does not induce any obvious phenotypes, in *ey>p35* eye discs it is sufficient to induce head capsule overgrowth (Figure 1V-X). Consistently, this is accompanied by the generation of ROS and hemocyte activation (Figure 2G,Q) as well as JNK activity and Wg expression (Figure S3). Taken together, under undead conditions, Myo1D is both necessary and sufficient for production of ROS which leads to activation of hemocytes, JNK and Wg signaling, resulting in AiP and tissue overgrowth.

The head, IQ and tail domains of Myo1D are required for ROS generation and AiP

As a myosin, Myo1D contains head (motor), neck (IQ) and tail regions (Figure 2A). We examined which domains of Myo1D function in AiP-induced overgrowth and tested *Myo1D* transgenes which mutate critical residues in the head region or delete neck and tail domains (Hozumi et al., 2008). Although these mutant transgenes are not expressed at comparable levels in *ey>hid,p35* background (Figure S4K), we were still able to obtain meaningful results. While expression of $Myo1D^{wt}$ strongly enhanced *ey>hid,p35*–induced head overgrowth (Figure 1I; Figure 2B, genotype 2), expression of constructs that mutate the ATP binding site ($Myo1D^{mATP\text{-}bs}$) or delete the Actin-binding site ($Myo1D^{\Delta Actin\text{-}bs}$) in the head region did not enhance *ey>hid,p35*-induced overgrowth (Figure 2B, genotypes 3,4) suggesting that the ATP-

hydrolyzing and Actin-binding activities of Myo1D are required for AiP-induced overgrowth. Strikingly, expression of *Myo1D* constructs that delete the neck (IQ) (*Myo1D*$^{\Delta IQ}$) and tail (*Myo1D*$^{\Delta tail}$) regions acted as strong suppressors of *ey>hid,p35*-induced overgrowth (Figure 2B, genotypes 5,6; Figure S4A-C) suggesting that these deletion constructs act as dominant negative alleles of *Myo1D*. These results imply that the IQ and tail domains of Myo1D play critical roles in AiP-induced overgrowth. Consistently, expression of *Myo1D*$^{\Delta IQ}$ in *ey>hid,p35* eye discs blocked the generation of ROS and the activation of hemocytes (Figure 2D,E,L,M).

Similar results were obtained when these transgenes were expressed in *ey>p35* discs. While expression of *Myo1D*^{wt} in *ey>p35* discs triggers overgrowth (Figure 1W,X), *Myo1D*$^{\Delta IQ}$ and *Myo1D*$^{\Delta tail}$ fail to do so (Figure S4G-J). Consistently, these mutant transgenes were unable to promote ROS generation and to activate hemocytes in *ey>p35* background (Figure 2H,R,S).

We also examined the ability of *Myo1D*^{wt}, *Myo1D*$^{\Delta IQ}$ and *Myo1D*$^{\Delta tail}$ transgenes to rescue (revert) the suppression of *ey>hid,p35*-induced overgrowth by *Myo1D*^{K2} and *Myo1D*^{Ey08899} mutants (Figure 1A,G,H). As expected, expression of *Myo1D*^{wt} strongly reverts the suppression of *ey>hid,p35* by *Myo1D*^{K2} and *Myo1D*^{Ey08899} mutants (Figure 2C, genotypes 3,4,7,8). In contrast, *Myo1D*$^{\Delta IQ}$ and *Myo1D*$^{\Delta tail}$ transgenes were not able to do so (Figure 2C, genotypes 5,6,9,10), providing further evidence for the critical role of the neck (IQ) and tail domains for Myo1D's function in AiP.

We also tested if expression of the second class I myosin, *Myo1C*, has a similar antagonistic function towards *Myo1D* for AiP as reported for L/R development (Hozumi et al., 2008; Petzoldt et al., 2012). Indeed, overexpression of *Myo1C* in *ey>hid,p35* discs weakly suppressed head capsule overgrowth and blocked generation of ROS and hemocyte activation (Figure 2B, genotype 7; Figure 2F,N; Figure S4D). Furthermore, ROS generation and hemocyte

activation by *Myo1D* in *ey>p35* discs is suppressed by simultaneous *Myo1C* expression (Figure 2I,T,U). These data support the notion that similar to L/R development, overexpression of *Myo1C* behaves in an antagonistic manner towards *Myo1D* in AiP.

Myo1D and Myo1C have a very similar domain structure (Morgan et al., 1995; Morgan et al., 1994; Okumura et al., 2015). We tested chimeras which swap the head with the neck (IQ) and tail regions of both proteins (*Myo1C*^{H}*-1D*$^{IQ\text{-}tail}$ and *Myo1D*^{H}*-1C*$^{IQ\text{-}tail}$) (Hozumi et al., 2008) in the undead AiP model. *Myo1C*^{H}*-1D*$^{IQ\text{-}tail}$ strongly enhances the overgrowth phenotype of *ey>hid,p35* flies similar to overexpression of *Myo1D*^{wt} (Figure 2B, genotype 8; Figure S4E). In contrast, the reverse chimera (*Myo1D*^{H}*-1C*$^{IQ\text{-}tail}$) weakly suppressed the overgrowth phenotype (Figure 2B, genotype 9; Figure S4F). Consistently, expression of *Myo1C*^{H}*-1D*$^{IQ\text{-}tail}$ in *ey>hid,p35* eye discs resulted in strong hemocyte activation at eye discs, while *Myo1D*^{H}*-1C*$^{IQ\text{-}tail}$ blocked hemocyte activation (Figure 2O,P). These data suggest that while the head (motor) domain is interchangeable between Myo1D and Myo1C, the specificity of Myo1D for overgrowth-promoting AiP lies in the neck (IQ) and tail domains of Myo1D.

Genetic and physical interaction between Myo1D and Dronc

Our observation that reduced Myo1D activity causes loss of ROS places Myo1D genetically between the initiator caspase Dronc and the NADPH oxidase Duox in the AiP pathway (Figure 1S,U). Therefore, we examined for a genetic and physical interaction between Dronc and Myo1D. While mis-expression of *Dronc* and *Myo1D* alone causes weak overgrowth of *ey>p35* head capsules, co-expression of both genes triggers very strong overgrowth (Figure 3A-D) suggesting that they genetically interact.

Therefore, we tested if the two proteins also physically interact. Because available Myo1D-specific antibodies failed in immunoprecipitation experiments, we expressed a *Myo1D-GFP* fusion protein in *ey>hid,p35* discs and immunoprecipitated Myo1D-GFP with GFP-conjugated beads. These immunoprecipitates contained endogenous Dronc protein (Figure 3E). In reverse experiments, we detected HA-tagged Myo1D in immunoprecipitates of Flag-Dronc from eye disc extracts (Figure 3F) suggesting that Myo1D and Dronc form a protein complex.

Because of the physical interaction, we considered that Myo1D is a proteolytic target of the caspase Dronc. However, while active Dronc is able to process its known substrate DrICE in cleavage assays *in vitro*, there is no detectable proteolytic event with Myo1D (Figure 3G). Furthermore, in immunoblots of protein extracts from undead *ey>hid,p35,Myo1D-GFP* eye discs, we did not detect a cleavage product of Myo1D-GFP even in the presence of an additional *dronc* transgene (Figure 3H). Therefore, although Dronc and Myo1D genetically and physically interact, Myo1D does not appear to be a proteolytic target of Dronc in undead cells.

Myo1D is required for membrane localization and stabilization of Dronc

To examine the physiological significance of the Dronc/Myo1D interaction, we performed immunolocalization studies of the two proteins in eye-antennal imaginal discs from 3rd instar larvae. The eye-antennal imaginal disc is composed of two epithelial sheets, the columnar cells of the disc proper (DP) and the squamous cells of the peripodial membrane (PM), that form a sac-like structure separated by a lumen (Figure 4A). In the following, we present the immunolocalization data in orthogonal sections as illustrated on the right of Figure 4A. In cells of control (*ey-Gal4*) eye imaginal discs, endogenous Myo1D is strongly expressed in PM cells and enriched at the basal side of the plasmamembrane of DP cells (Figure 4B; arrows).

Endogenous Dronc protein is also strongly expressed in PM cells, while in DP cells, it is present in the cytosol with a weak plasmamembrane localization at the basal side of the disc (Figure 4B'). *Myo1D* RNAi disrupts the membrane localization of Dronc (Figure 4C'). Importantly, in undead *ey>hid,p35* discs, endogenous Dronc protein becomes strongly enriched at the plasmamembrane of DP cells (Figure 4D'). Co-labeling with the polarity marker Dlg suggests that Dronc is specifically localized to the basal side of the plasmamembrane in DP cells matching the localization of Myo1D (Figure 4D). This membrane localization is dependent on Myo1D, because in *ey>hid,p35* discs expressing *Myo1D* RNAi, Dronc protein loses the membrane localization (Figure 4E'). These differences in the localization of Dronc to the basal side of the plasmamembrane of DP cells are quantified in Figure 4F. Furthermore, *Myo1D* RNAi appears to result in a reduction of the protein level of Dronc (Figure 4F') suggesting that Myo1D-dependent membrane localization also stabilizes Dronc protein in undead cells. This is confirmed by immunoblot analysis (Figure 4G).

It was recently reported that Dronc localizes to the plasmamembrane of larval salivary gland (SG) cells which is dependent on another factor, Tango7 (Kang et al., 2017). SGs are composed of secretory, columnar epithelial cells which form a tube with a lumen inside (Andrew et al., 2000). The apical membranes of SG cells face the lumen, while the basal side of SG cells is exposed to the exterior of the gland (Figure 4H). Because the *ey-Gal4* driver is also expressed in SG cells, we examined the dependence of the membrane localization of Dronc on Myo1D in SG cells. In sections (Figure 4H, bottom) of control (*ey-Gal4*) SG cells, endogenous Dronc protein localizes at the plasmamembrane consistent with (Kang et al., 2017) as does Myo1D (Figure 4I-I''). Similar to eye discs, this localization occurs at the basal side of the plasmamembrane, as judged by co-localization with the polarity marker Dlg (Figure 4I'',I'''). In

contrast to eye discs, *Myo1D* RNAi does not significantly disturb the Dronc localization in control SG cells (Figure 4J). This is likely due to Tango7, a factor that is required for membrane localization of Dronc in SGs (Kang et al., 2017). Importantly, in undead (*ey>hid,p35*) SGs, the localization of endogenous Dronc to the basal side of the plasmamembrane is strongly increased (Figure 4K). This increased membrane localization of Dronc in undead SG cells is dependent on Myo1D, as *Myo1D* RNAi strongly reduces it (Figure 4L).

Furthermore, ectopically targeting Myo1D-GFP to the apical surface of DP cells by co-expression with *GrabFP-A$_{Int}$* which traps GFP fusion proteins to the apical side of epithelial cells (Harmansa et al., 2017) disrupts the basal localization of Dronc protein in undead cells (Figure S5). Combined, these data establish that Myo1D is required for localization of Dronc to the basal side of the plasmamembrane of undead epithelial and SG cells.

In *ey>hid,p35* eye imaginal discs, mis-expression of *Myo1D^{wt}* also triggers strong enrichment of endogenous Dronc at the basal plasmamembrane of DP cells (Figure 4M,M'). In Figure 2, we established that the neck (IQ) and tail domains of Myo1D determine its specificity in AiP. Therefore, we examined the role of the IQ and tail domains for membrane localization of both Dronc and Myo1D. The localization of Dronc to the basal membrane is at least partially lost by expression of *Myo1D$^{\Delta IQ}$* and *Myo1D$^{\Delta tail}$* (Figure 4P-O'). Although *Myo1D$^{\Delta IQ}$* is expressed in very low levels by *ey-hid,p35* (Figure S4K), the protein levels of Dronc at the plasmamembrane are strongly reduced (Figure 4N,N'; quantified in Figure 4P). Myo1D$^{\Delta tail}$ has lost its membrane association completely and consequently Dronc has a large cytosolic localization (Figure 4O,O';P). These findings suggest that the IQ domain of Myo1D is involved in the interaction with Dronc, while the tail domain mediates the association with the plasmamembrane.

Because the adaptor protein Dark recruits Dronc into the apoptosome during apoptosis, we analyzed the subcellular localization of Dark in SGs. Because of the lack of suitable Dark antibodies, we expressed a GFP-tagged Dark (Dark-GFP) construct in SGs and examined the localization of Dark-GFP using a GFP antibody. In contrast to Dronc protein, the overall localization of Dark-GFP does not change in undead SGs and is not dependent on *Myo1D* (Figure S6A-C). Although there is a membrane-associated component of Dark-GFP, it is largely cytosolic and there is only very weak colocalization with Dronc in undead SGs (Figure S6D). Therefore, the sequestration of Dronc to the basal side of the plasmamembrane may suggest a mechanism by which Dronc is largely separated from its apoptotic partner Dark.

Membrane-localized Dronc triggers non-apoptotic caspase activity at the membrane

In normal apoptotic cells of imaginal discs, Dronc triggers caspase activation in the cytosol as visualized by cleaved caspase (CC3) antibody labeling both in surface views and in orthogonal sections (Figure 5A). Therefore, we examined if membrane-localized Dronc in undead cells is also able to trigger CC3 labeling. Indeed, in undead (*ey>hid,p35)* eye discs, we detect CC3 labeling and similar to Dronc, it is largely localized at the plasmamembrane, overlapping with Myo1D (Figure 5B-B’’). In orthogonal sections, CC3 is localized to PM cells as well as to the basal plasmamembrane of undead DP cells, similar to Myo1D (Figure 5B’’’,5B’’’’) and Dronc (Figure 4D). In undead wing imaginal discs (*nub>hid,p35*), we also observe a membrane localization of CC3 at the basal side of DP cells (Figure S1I, inset). The membrane localization of CC3 labeling in undead DP cells is dependent on Myo1D as *Myo1D* RNAi disrupts the localized labeling of CC3 at the plasmamembrane (Figure 5C) consistent with the dependence of Dronc on Myo1D for membrane localization (Figure 4E).

Likewise, in undead (*ey>hid,p35*) SG cells, there is enriched CC3 labeling at the basal side of the plasmamembrane (Figure 5D',D'''). Even under normal conditions (without expression of *hid* and *p35*), can we detect membrane-localized CC3 labeling in SG cells (Figure 5F,F'), but it is much weaker than in undead cells. Knockdown of *Myo1D* strongly reduces CC3 labeling at the plasmamembrane of both normal and undead SG cells (Figure 5E,G) suggesting that *Myo1D* is required for Dronc activity at the plasmamembrane.

Interestingly, the SGs analyzed in Figure 5D,E were obtained from 3rd instar larvae and are not apoptotic at that stage. That raises the possibility that the caspase activity at the plasmamembrane is non-apoptotic in nature. To examine this possibility, we employed differential labeling specificities of CC3 and cleaved Dcp1 (cDcp1) antibodies. We have previously shown that CC3 labeling detects both apoptotic and non-apoptotic activity of Dronc (Figure 5H) (Fan and Bergmann, 2010). Consistently, membrane-localized CC3 labeling in SGs is completely dependent on Dronc, as it disappears in homozygous *dronc* mutants (Figure 5I). In contrast to CC3 antibody, the cDcp1 antibody was raised to specifically detect a neo-epitope of Dcp1 after Dronc cleavage and is a more specific marker for Dronc's apoptotic activity (Figure 5H). *dcp1;drICE* double null mutants completely lack apoptosis (Fan and Bergmann, 2010) and consistently, these double mutant SGs do not label with the cDcp1 antibody (Figure 5J). In contrast, membrane-localized CC3 labeling is still present in *dcp1;drICE* double null SGs (Figure 5K), further supporting the notion that the membrane localized CC3 activity is non-apoptotic. Combined, these data demonstrate that membrane-localized Dronc has a non-apoptotic activity and suggest that the plasmamembrane, specifically the basal side of the plasmamembrane, acts as a non-apoptotic compartment.

Myo1D-induced ROS generation depends on the NADPH oxidase Duox and Dronc

We showed previously that Duox generates eROS in the undead AiP model which is required for hemocyte recruitment and overgrowth (Fogarty et al., 2016). We therefore examined if Myo1D's ability to induce ROS generation, hemocyte recruitment and overgrowth of *ey>p35,Myo1D* flies (Figure 6A-C) is dependent on Duox. Indeed, knockdown of *Duox* suppresses ROS production, hemocyte activation and overgrowth of *ey>p35,Myo1D* eye discs (Figure 6D-F; quantified in G,H) suggesting that Duox mediates the overgrowth-promoting function of Myo1D.

We also found that endogenous Duox and Dronc proteins co-localize at the basal side of the plasmamembrane of undead DP cells in imaginal discs and SG cells (Figure 6I-N). Excitingly, while Duox mis-expression alone is unable to induce ROS in *ey>p35* epithelial cells, co-expression of Duox and Myo1D strongly increases the ability of Duox to generate ROS (Figure 6O-R; quantified in 6S). These findings suggest that Myo1D directly or indirectly promotes the activation of Duox for eROS generation.

Interestingly, reduction of *dronc* activity by RNAi in *ey>p35* eye discs suppresses both *Myo1D*-induced overgrowth and ROS generation (Figure 6T,U; compare to Figure 6A,B,Q). This result suggests that Dronc has an important function at the plasmamembrane for ROS generation and AiP, and that Myo1D enables Dronc to exert this function by localizing it to the membrane.

Myo1D is required for neoplastic growth of *scrib$^{-/-}$Ras^{V12}* through control of ROS production

Recently, we showed that neoplastic growth and invasive behavior of epithelial *scrib$^{-/-}$ Ras^{V12}* disc cells in *Drosophila* is dependent on caspase-generated ROS (Perez et al., 2017). Furthermore, in the presence of *Ras^{V12}*, *scrib$^{-/-}$* and other tumor cells acquire undead properties (Hirabayashi et al., 2013; Perez et al., 2017). Therefore, given the involvement of Myo1D in ROS generation and overgrowth in the undead AiP model, we examined if *Myo1D* is required for the neoplastic phenotype of *scrib$^{-/-}$Ras^{V12}*. In mosaic eye imaginal discs, *scrib$^{-/-}$Ras^{V12}* clones occupy up to 90% of the tissue (Figure 7A,C) (Brumby and Richardson, 2003; Pagliarini and Xu, 2003). Reducing *Myo1D* levels by RNAi significantly reduces the size of *scrib$^{-/-}$ Ras^{V12}* clones (Figure 7B,C). Furthermore, *scrib$^{-/-}$ Ras^{V12}* cells from eye discs display metastatic behavior and invade distant tissue such as the ventral nerve cord (VNC) in the larval brain (Figure 7D, arrow) (Pagliarini and Xu, 2003). Reducing *Myo1D* activity by RNAi suppresses the invasive behavior of *scrib$^{-/-}$Ras^{V12}* cells and normalizes their growth (Figure 7E,F). These observations suggest that *Myo1D* is required for neoplastic growth and invasive behavior of *scrib$^{-/-}$Ras^{V12}* mutant cells.

Because ROS generation in *scrib$^{-/-}$ Ras^{V12}* mosaic discs is dependent on caspases and Duox (Perez et al., 2017) similar to the undead AiP model, we examined ROS levels in *scrib$^{-/-}$ Ras^{V12}* discs after knockdown of *Myo1D*. Indeed, loss of *Myo1D* results in strong reduction of DHE labeling (Figure 7G-I) suggesting that *Myo1D* is required for ROS generation. As a consequence of ROS reduction, hemocytes are no longer activated and display the naïve morphology in *scrib$^{-/-}$Ras^{V12};Myo1D^{RNAi}* mosaic discs (Figure 7J-L).

Because we showed in the undead (*ey>hid,p35*) model that Dronc is localized to the plasmamembrane (Figure 4) and because *Ras^{V12}* confers undead properties to tumor cells

(Hirabayashi et al., 2013; Perez et al., 2017), we examined the subcellular localization of Dronc in *scrib*$^{-/-}$*Ras*^{V12} mutant cells. Similar to the *ey>hid,p35* model, Dronc appears to be enriched at the plasmamembrane in *scrib*$^{-/-}$*Ras*^{V12} mutant cells (Figure 7M,M'). Upon knockdown of *Myo1D*, the membrane localization of Dronc is disrupted and Dronc protein levels are reduced (Figure 7N,N'). In summary, it appears that the mechanism of Myo1D function in the undead AiP and the neoplastic *scrib*$^{-/-}$*Ras*^{V12} models are very similar. In both cases, Myo1D translocates Dronc to the plasmamembrane where is stimulates Duox activation in a non-apoptotic function.

Discussion

In this paper, we identified a novel function of the class I unconventional myosin, Myo1D. In addition to its established function as a L/R determinant (Hozumi et al., 2006; Speder et al., 2006), Myo1D also plays an essential role in AiP. Mechanistically, we found that Myo1D is involved in the localization of the initiator caspase Dronc to the basal side of the plasmamembrane of undead DP disc and SG cells (Figure 4). Myo1D interacts with Dronc suggesting that it may directly translocate Dronc to the plasmamembrane. However, Myo1D does not appear to be a cleavage target of the caspase Dronc.

The observed localization of Dronc to the basal side of the plasmamembrane in undead disc proper (DP) cells is critical for the mechanism of AiP. Undead cells attract hemocytes to the discs in a Dronc- and Duox-dependent manner (Fogarty et al., 2016). However, that occurs at the basal side of DP cells of imaginal discs because the basal side is exposed to the hemolymph which contains circulating hemocytes, while the apical side faces the lumen between the DP and the PM (Figure 4A). Consistently, there is also an enrichment of Duox at the basal side of the plasmamembrane (Figure 6I,K). Therefore, in order to be able to activate Duox for ROS

generation and hemocyte activation, Dronc needs to be specifically present at the basal side of the plasma membrane (Figure 8).

It has long been known that caspases, including Dronc, have non-apoptotic functions in addition to their well characterized role in apoptosis (Aram et al., 2016; Aram et al., 2017; Fogarty and Bergmann, 2017; Fogarty et al., 2016; Mukherjee and Williams, 2017; Nakajima and Kuranaga, 2017; Shalini et al., 2015). In this paper, we reveal one mechanism by which cells may activate a caspase (Dronc) without the detrimental consequences of apoptosis. The sequestration of Dronc to the basal side of the plasmamembrane in a Myo1D-dependent manner and the low abundance of Dronc's apoptotic partner Dark at the plasmamembrane (Figure S6) may ensure localized and controlled apoptosome activity which is sufficient for AiP, but not for killing cells. Alternatively, apoptotic substrates needed for the execution of apoptosis may not be present at the plasmamembrane or in insufficient amount to pass the apoptotic threshold.

While we addressed the role of membrane localization of Dronc under undead conditions, recently membrane-localized Dronc was shown in SGs under normal conditions (Kang et al., 2017) which explains the membrane localization of Dronc at control SGs (Figure 4I). Here, membrane-localized Dronc is required for F-actin cytoskeleton dismantling at the end of larval development in a non-apoptotic manner (Kang et al., 2017). In addition to the plasmamembrane, the outer mitochondrial membrane has been shown to provide a non-apoptotic platform for caspase activation, in this case during sperm maturation (Aram et al., 2016). Therefore, membranes in general may provide a local environment for non-apoptotic caspase activities.

The membrane localization of Dronc in SGs is mediated by Tango7 which has previously been implicated in spermatid maturation (D'Brot et al., 2013; Kang et al., 2017). As mentioned above, membrane-localized Dronc is required for dismantling of cortical F-actin cytoskeleton in

SGs of late larvae (Kang et al., 2017). However, while *Tango7* RNAi blocks actin dismantling, *Myo1D* RNAi does not (data not shown) suggesting that the roles of Tango7 and Myo1D for membrane-localization of Dronc are different from each other. That also explains why in undead SGs the membrane localization of Dronc strongly increases in a *Myo1D*-dependent manner (Figure 4K). Unfortunately, we were not able to test if Tango7 is involved in AiP. *Tango7* RNAi in eye imaginal discs results in complete loss of the disc. *Tango7* encodes the homolog of eukaryotic translation initiation factor 3m (eIF3m) suggesting that it may also have an important requirement for protein translation, explaining the loss of the eye disc by *Tango7* RNAi.

In addition to Myo1D and Tango7, there is at least one other factor, Crinkled (Ck), that directs Dronc to non-apoptotic functions. Ck bridges the interaction between Dronc and the kinase Shaggy/GSK-β, resulting in the selective activation of Shaggy/GSK-β which then promotes non-apoptotic activities such as the specification of scutellar bristles, border cell migration and correct branching of the aristae (Orme et al., 2016). Interestingly, *Ck* encodes another unconventional myosin, a member of the class VII myosin family (Orme et al., 2016) potentially suggesting that other myosins may also direct non-apoptotic functions to caspases.

Myo1D and the apoptotic machinery have been linked to male terminalia rotation, a L/R process during pupal development (Abbott and Lengyel, 1991; Grether et al., 1995; Krieser et al., 2007; Macias et al., 2004; Muro et al., 2006). Indeed, apoptosis is required for Myo1D-dependent male terminalia rotation (Kuranaga et al., 2011; Suzanne et al., 2010). It is unknown how Myo1D interacts with the apoptotic machinery to direct this L/R movement. In future studies, it will be interesting to examine if the Myo1D-dependent mechanism identified here for AiP also applies to male terminalia rotation or whether a separate mechanism exists in this context.

Myo1D not only localizes Dronc to the plasmamembrane, it also stabilizes it (Figure 4E',G). Dronc is activated in undead cells and activated Dronc is subject of increased protein degradation (Lee et al., 2011; Lee et al., 2016; Shapiro et al., 2008). Thus, Myo1D prevents degradation of Dronc by changing its subcellular localization to the plasmamembrane.

Myo1D has a very strong requirement in AiP in the undead model, and a requirement in the *scrib*$^{-/-}$*Ras*^{V12} tumorigenesis model, yet it does not appear to play any significant role in genuine AiP (data not shown). In fact, Myo1D is the first gene identified that is essential for the hyper-proliferation of undead AiP, but not required for the regeneration of genuine AiP. The mechanism revealed in this paper provides an explanation for this behavior. During genuine AiP, cells are allowed to undergo apoptosis, which requires cytosolic Dronc activity. Although ROS are generated during genuine AiP (Santabarbara-Ruiz et al., 2015), the origin of these ROS has not been determined and may not require the plasmamembrane-localized Duox. Therefore, a key difference between genuine AiP and undead AiP, and potentially between other regenerative versus tumorigenic models, may be the altered localization of Dronc to a non-apoptotic compartment at the plasmamembrane, and a shift from balanced apoptosis and proliferation, to dominant proliferation. The next big question will be to examine what exactly is prompting Myo1D to drive this re-localization of Dronc under sustained undead conditions, but not under the limited regenerative conditions of the genuine AiP models, and whether that answer provides any insight into the cancer versus wound healing models.

In conclusion, in addition to its role in L/R development, we identified a novel function of Myo1D for AiP and tumorigenesis. We also identified the basal side of the plasmamembrane as a non-apoptotic environment for caspase function. In future work, it will be important to identify the mechanisms by which Dronc mediates its non-apoptotic functions at the

plasmamembrane for AiP and other cellular processes that require membrane-localization of Dronc and other caspases.

Acknowledgement

We would like to thank István Andó, Takahiro Chihara, Georg Halder, Bruce Hay, Madhuri Kango-Singh, Won Jae Lee, Kenji Matsuno, Kim McCall, Pascal Meier, Masayuki Miura, Stéphane Noselli, Guy Salvesen, Hermann Steller, the Bloomington *Drosophila* Stock Center, the Vienna *Drosophila* Resource Center (VDRC) and the Developmental Studies Hybridoma Bank (DSHB) for reagents, antibodies and fly stocks. This work was funded by the National Institute of General Medical Science (NIGMS) under award number R35GM118330. The content is solely the responsibility of the authors and does not necessarily represent the official views of the National Institutes of Health.

Author Contributions

AA performed most of the experiments; SW and YF identified Myo1D as suppressor of AiP; CEF performed *in vitro* cleavage assays; JLL performed experiments with genuine AiP; AB and AA designed the experiments and wrote the manuscript; AB secured funding.

Declaration of Interests

The authors declare no competing interests.

References

Abbott, M.K., and Lengyel, J.A. (1991). Embryonic head involution and rotation of male terminalia require the Drosophila locus head involution defective. Genetics *129*, 783-789.

Andrew, D.J., Henderson, K.D., and Seshaiah, P. (2000). Salivary gland development in Drosophila melanogaster. Mech Dev *92*, 5-17.

Aram, L., Braun, T., Braverman, C., Kaplan, Y., Ravid, L., Levin-Zaidman, S., and Arama, E. (2016). A Krebs Cycle Component Limits Caspase Activation Rate through Mitochondrial Surface Restriction of CRL Activation. Developmental cell *37*, 15-33.

Aram, L., Yacobi-Sharon, K., and Arama, E. (2017). CDPs: caspase-dependent non-lethal cellular processes. Cell Death Differ *24*, 1307-1310.

Barylko, B., Binns, D.D., and Albanesi, J.P. (2000). Regulation of the enzymatic and motor activities of myosin I. Biochimica et biophysica acta *1496*, 23-35.

Brumby, A.M., and Richardson, H.E. (2003). scribble mutants cooperate with oncogenic Ras or Notch to cause neoplastic overgrowth in Drosophila. EMBO J *22*, 5769-5779.

Chera, S., Ghila, L., Dobretz, K., Wenger, Y., Bauer, C., Buzgariu, W., Martinou, J.C., and Galliot, B. (2009). Apoptotic cells provide an unexpected source of Wnt3 signaling to drive hydra head regeneration. Developmental cell *17*, 279-289.

Coluccio, L.M. (1997). Myosin I. The American journal of physiology *273*, C347-359.

Coutelis, J.B., Gonzalez-Morales, N., Geminard, C., and Noselli, S. (2014). Diversity and convergence in the mechanisms establishing L/R asymmetry in metazoa. EMBO reports *15*, 926-937.

D'Brot, A., Chen, P., Vaishnav, M., Yuan, S., Akey, C.W., and Abrams, J.M. (2013). Tango7 directs cellular remodeling by the Drosophila apoptosome. Genes Dev *27*, 1650-1655.

Fan, Y., and Bergmann, A. (2008a). Apoptosis-induced compensatory proliferation. The Cell is dead. Long live the Cell! Trends Cell Biol *18*, 467-473.

Fan, Y., and Bergmann, A. (2008b). Distinct mechanisms of apoptosis-induced compensatory proliferation in proliferating and differentiating tissues in the Drosophila eye. Developmental cell *14*, 399-410.

Fan, Y., and Bergmann, A. (2010). The cleaved-Caspase-3 antibody is a marker of Caspase-9-like DRONC activity in Drosophila. Cell Death Differ *17*, 534-539.

Fan, Y., and Bergmann, A. (2014). Multiple mechanisms modulate distinct cellular susceptibilities toward apoptosis in the developing Drosophila eye. Developmental cell *30*, 48-60.

Fan, Y., Wang, S., Hernandez, J., Yenigun, V.B., Hertlein, G., Fogarty, C.E., Lindblad, J.L., and Bergmann, A. (2014). Genetic models of apoptosis-induced proliferation decipher activation of JNK and identify a requirement of EGFR signaling for tissue regenerative responses in Drosophila. PLoS Genet *10*, e1004131.

Fogarty, C.E., and Bergmann, A. (2015). The Sound of Silence: Signaling by Apoptotic Cells. Curr Top Dev Biol *114*, 241-265.

Fogarty, C.E., and Bergmann, A. (2017). Killers creating new life: caspases drive apoptosis-induced proliferation in tissue repair and disease. Cell Death Differ *24*, 1390-1400.

Fogarty, C.E., Diwanji, N., Lindblad, J.L., Tare, M., Amcheslavsky, A., Makhijani, K., Bruckner, K., Fan, Y., and Bergmann, A. (2016). Extracellular Reactive Oxygen Species Drive Apoptosis-Induced Proliferation via Drosophila Macrophages. Curr Biol *26*, 575-584.

Geminard, C., Gonzalez-Morales, N., Coutelis, J.B., and Noselli, S. (2014). The myosin ID pathway and left-right asymmetry in Drosophila. Genesis *52*, 471-480.

Glise, B., Bourbon, H., and Noselli, S. (1995). hemipterous encodes a novel Drosophila MAP kinase kinase, required for epithelial cell sheet movement. Cell *83*, 451-461.

Grether, M.E., Abrams, J.M., Agapite, J., White, K., and Steller, H. (1995). The head involution defective gene of Drosophila melanogaster functions in programmed cell death. Genes Dev *9*, 1694-1708.

Harmansa, S., Alborelli, I., Bieli, D., Caussinus, E., and Affolter, M. (2017). A nanobody-based toolset to investigate the role of protein localization and dispersal in Drosophila. eLife *6*.

Hayashi, T., and Murakami, R. (2001). Left-right asymmetry in Drosophila melanogaster gut development. Dev Growth Differ *43*, 239-246.

Herrera, S.C., Martin, R., and Morata, G. (2013). Tissue homeostasis in the wing disc of Drosophila melanogaster: immediate response to massive damage during development. PLoS Genet *9*, e1003446.

Hirabayashi, S., Baranski, T.J., and Cagan, R.L. (2013). Transformed Drosophila cells evade diet-mediated insulin resistance through wingless signaling. Cell *154*, 664-675.

Holland, P.M., Suzanne, M., Campbell, J.S., Noselli, S., and Cooper, J.A. (1997). MKK7 is a stress-activated mitogen-activated protein kinase kinase functionally related to hemipterous. The Journal of biological chemistry *272*, 24994-24998.

Hozumi, S., Maeda, R., Taniguchi-Kanai, M., Okumura, T., Taniguchi, K., Kawakatsu, Y., Nakazawa, N., Hatori, R., and Matsuno, K. (2008). Head region of unconventional myosin I family members is responsible for the organ-specificity of their roles in left-right polarity in Drosophila. Developmental dynamics : an official publication of the American Association of Anatomists *237*, 3528-3537.

Hozumi, S., Maeda, R., Taniguchi, K., Kanai, M., Shirakabe, S., Sasamura, T., Speder, P., Noselli, S., Aigaki, T., Murakami, R.*, et al.* (2006). An unconventional myosin in Drosophila reverses the default handedness in visceral organs. Nature *440*, 798-802.

Huh, J.R., Guo, M., and Hay, B.A. (2004). Compensatory proliferation induced by cell death in the Drosophila wing disc requires activity of the apical cell death caspase Dronc in a nonapoptotic role. Curr Biol *14*, 1262-1266.

Kamber Kaya, H.E., Ditzel, M., Meier, P., and Bergmann, A. (2017). An inhibitory mono-ubiquitylation of the Drosophila initiator caspase Dronc functions in both apoptotic and non-apoptotic pathways. PLoS Genet *13*, e1006438.

Kang, Y., Neuman, S.D., and Bashirullah, A. (2017). Tango7 regulates cortical activity of caspases during reaper-triggered changes in tissue elasticity. Nat Commun *8*, 603.

Krieser, R.J., Moore, F.E., Dresnek, D., Pellock, B.J., Patel, R., Huang, A., Brachmann, C., and White, K. (2007). The Drosophila homolog of the putative phosphatidylserine receptor functions to inhibit apoptosis. Development *134*, 2407-2414.

Kuranaga, E., Matsunuma, T., Kanuka, H., Takemoto, K., Koto, A., Kimura, K., and Miura, M. (2011). Apoptosis controls the speed of looping morphogenesis in Drosophila male terminalia. Development *138*, 1493-1499.

Kurucz, E., Vaczi, B., Markus, R., Laurinyecz, B., Vilmos, P., Zsamboki, J., Csorba, K., Gateff, E., Hultmark, D., and Ando, I. (2007). Definition of Drosophila hemocyte subsets by cell-type specific antigens. Acta biologica Hungarica *58 Suppl*, 95-111.

Lee, T.V., Fan, Y., Wang, S., Srivastava, M., Broemer, M., Meier, P., and Bergmann, A. (2011). Drosophila IAP1-mediated ubiquitylation controls activation of the initiator caspase DRONC independent of protein degradation. PLoS Genet *7*, e1002261.

Lee, T.V., Kamber Kaya, H.E., Simin, R., Baehrecke, E.H., and Bergmann, A. (2016). The initiator caspase Dronc is subject of enhanced autophagy upon proteasome impairment in Drosophila. Cell Death Differ *23*, 1555-1564.

Li, F., Huang, Q., Chen, J., Peng, Y., Roop, D.R., Bedford, J.S., and Li, C.Y. (2010). Apoptotic cells activate the "phoenix rising" pathway to promote wound healing and tissue regeneration. Sci Signal *3*, ra13.

Ligoxygakis, P., Strigini, M., and Averof, M. (2001). Specification of left-right asymmetry in the embryonic gut of Drosophila. Development *128*, 1171-1174.

Macias, A., Romero, N.M., Martin, F., Suarez, L., Rosa, A.L., and Morata, G. (2004). PVF1/PVR signaling and apoptosis promotes the rotation and dorsal closure of the Drosophila male terminalia. The International journal of developmental biology *48*, 1087-1094.

Martin, F.A., Perez-Garijo, A., and Morata, G. (2009). Apoptosis in Drosophila: compensatory proliferation and undead cells. The International journal of developmental biology *53*, 1341-1347.

Mollereau, B., Perez-Garijo, A., Bergmann, A., Miura, M., Gerlitz, O., Ryoo, H.D., Steller, H., and Morata, G. (2013). Compensatory proliferation and apoptosis-induced proliferation: a need for clarification. Cell Death Differ *20*, 181.

Morgan, N.S., Heintzelman, M.B., and Mooseker, M.S. (1995). Characterization of myosin-IA and myosin-IB, two unconventional myosins associated with the Drosophila brush border cytoskeleton. Developmental biology *172*, 51-71.

Morgan, N.S., Skovronsky, D.M., Artavanis-Tsakonas, S., and Mooseker, M.S. (1994). The molecular cloning and characterization of Drosophila melanogaster myosin-IA and myosin-IB. Journal of molecular biology *239*, 347-356.

Mukherjee, A., and Williams, D.W. (2017). More alive than dead: non-apoptotic roles for caspases in neuronal development, plasticity and disease. Cell Death Differ *24*, 1411-1421.

Muro, I., Berry, D.L., Huh, J.R., Chen, C.H., Huang, H., Yoo, S.J., Guo, M., Baehrecke, E.H., and Hay, B.A. (2006). The Drosophila caspase Ice is important for many apoptotic cell deaths and for spermatid individualization, a nonapoptotic process. Development *133*, 3305-3315.

Nakajima, Y.I., and Kuranaga, E. (2017). Caspase-dependent non-apoptotic processes in development. Cell Death Differ *24*, 1422-1430.

Okumura, T., Sasamura, T., Inatomi, M., Hozumi, S., Nakamura, M., Hatori, R., Taniguchi, K., Nakazawa, N., Suzuki, E., Maeda, R.*, et al.* (2015). Class I myosins have overlapping and specialized functions in left-right asymmetric development in Drosophila. Genetics *199*, 1183-1199.

Orme, M.H., Liccardi, G., Moderau, N., Feltham, R., Wicky-John, S., Tenev, T., Aram, L., Wilson, R., Bianchi, K., Morris, O.*, et al.* (2016). The unconventional myosin CRINKLED and its mammalian orthologue MYO7A regulate caspases in their signalling roles. Nat Commun *7*, 10972.

Pagliarini, R.A., and Xu, T. (2003). A genetic screen in Drosophila for metastatic behavior. Science *302*, 1227-1231.

Perez-Garijo, A., Martin, F.A., and Morata, G. (2004). Caspase inhibition during apoptosis causes abnormal signalling and developmental aberrations in Drosophila. Development *131*, 5591-5598.

Perez, E., Lindblad, J.L., and Bergmann, A. (2017). Tumor-promoting function of apoptotic caspases by an amplification loop involving ROS, macrophages and JNK in Drosophila. eLife *6*.

Petzoldt, A.G., Coutelis, J.B., Geminard, C., Speder, P., Suzanne, M., Cerezo, D., and Noselli, S. (2012). DE-Cadherin regulates unconventional Myosin ID and Myosin IC in Drosophila left-right asymmetry establishment. Development *139*, 1874-1884.

Rousset, R., Bono-Lauriol, S., Gettings, M., Suzanne, M., Speder, P., and Noselli, S. (2010). The Drosophila serine protease homologue Scarface regulates JNK signalling in a negative-feedback loop during epithelial morphogenesis. Development *137*, 2177-2186.

Ryoo, H.D., Gorenc, T., and Steller, H. (2004). Apoptotic cells can induce compensatory cell proliferation through the JNK and the Wingless signaling pathways. Developmental cell *7*, 491-501.

Salvesen, G.S., Hempel, A., and Coll, N.S. (2016). Protease signaling in animal and plant-regulated cell death. The FEBS journal *283*, 2577-2598.

Santabarbara-Ruiz, P., Lopez-Santillan, M., Martinez-Rodriguez, I., Binagui-Casas, A., Perez, L., Milan, M., Corominas, M., and Serras, F. (2015). ROS-Induced JNK and p38 Signaling Is Required for Unpaired Cytokine Activation during Drosophila Regeneration. PLoS Genet *11*, e1005595.

Shalini, S., Dorstyn, L., Dawar, S., and Kumar, S. (2015). Old, new and emerging functions of caspases. Cell Death Differ *22*, 526-539.

Shapiro, P.J., Hsu, H.H., Jung, H., Robbins, E.S., and Ryoo, H.D. (2008). Regulation of the Drosophila apoptosome through feedback inhibition. Nat Cell Biol *10*, 1440-1446.

Smith-Bolton, R.K., Worley, M.I., Kanda, H., and Hariharan, I.K. (2009). Regenerative growth in Drosophila imaginal discs is regulated by Wingless and Myc. Developmental cell *16*, 797-809.

Speder, P., Adam, G., and Noselli, S. (2006). Type ID unconventional myosin controls left-right asymmetry in Drosophila. Nature *440*, 803-807.

Suzanne, M., Petzoldt, A.G., Speder, P., Coutelis, J.B., Steller, H., and Noselli, S. (2010). Coupling of apoptosis and L/R patterning controls stepwise organ looping. Curr Biol *20*, 1773-1778.

Tseng, A.S., Adams, D.S., Qiu, D., Koustubhan, P., and Levin, M. (2007). Apoptosis is required during early stages of tail regeneration in Xenopus laevis. Developmental biology *301*, 62-69.

Tzolovsky, G., Millo, H., Pathirana, S., Wood, T., and Bownes, M. (2002). Identification and phylogenetic analysis of Drosophila melanogaster myosins. Molecular biology and evolution *19*, 1041-1052.

Yuan, S., and Akey, C.W. (2013). Apoptosome structure, assembly, and procaspase activation. Structure *21*, 501-515.

Figure legends

Figure 1. *Myo1D* is required for undead tissue overgrowth upstream of ROS production.

(**A**) Quantification of the suppression of head overgrowth of *ey>hid,p35* animals by *Myo1D* RNAi or *Myo1D* mutants as shown in (C-H). Displayed is also the enhancement by *Myo1D* misexpression (I). Suppression is determined based on a shift in the percentage from overgrown animals to wild-type. Details to statistics in this and all other figures can be found in STAR Methods. 50-150 flies were counted per genotype.

(**B**) The head capsule of a wild type fly. Scale bar: 200µm.

(**C,D**) Head capsule overgrowth of *ey>hid,p35* animals (C) is not suppressed by a control *UAS-empty vector* (*UAS-EV*) transgene (D).

(**E-H**) Representative examples of the suppression of *ey>hid,p35*-induced head overgrowth by *Myo1D* RNAi (E,F) and *Myo1D* mutants (G,H). $Myo1D^{RNAi(KK)}$ in (E) is VDRC line KK102456, $Myo1D^{RNAi(BL)}$ in (F) is Bloomington line BL33971. $Myo1D^{Ey}$ in (H) is $Myo1D^{Ey08859}$.

(**I**) Strong enhancement of the overgrowth phenotype of *ey>hid,p35* animals by *Myo1D* misexpression.

(**J-L'**) Eye imaginal discs of the indicated genotypes labeled for β-Gal (red, to visualize JNK activity), cleaved caspase3 (CC3, green) and ELAV (blue) which marks photoreceptor neurons in the posterior half of the disc. Scale bar: 50µm.

(**M-O'**) Hemocyte labeling using anti-NimrodC (NimC) antibody (Kurucz et al., 2007) of eye imaginal discs of indicated genotype. Arrows in (N') indicate cytoplasmic protrusions of activated hemocytes. Scale bars in (N): 50µm; in (N'): 20µm.

(**P**) Quantification of the NimC labelings in (M-O). NimC signal intensity was determined across the entire discs.

(**Q-S**) DHE labeling as ROS marker of imaginal discs of the same genotypes as in (M-O). Scale bar: 50µm.

(**T**) Quantification of DHE labelings in (Q-S). DHE signal intensity was determined across the entire discs.

(**U**) Schematic summary of the placement of Myo1D into the AiP pathway.

(**V-X**) Misexpression of *Myo1D* in *ey>p35* animals triggers head capsule overgrowth (W). Quantified in (X).

Figure 2. The neck (IQ) and tail regions of Myo1D are critical for AiP

(A) Outline of the domain structure of Myo1D. P = P-loop; s1/2 = switch1/2-loop.

(**B**) Summary of the head phenotypes of *ey>hid,p35* animals expressing the transgenes numbered and listed on the right. All *Myo1D* transgenes carry a HA-tag at the C-terminus.

(**C**) Summary of the rescue experiments of $Myo1D^{K2}$ and $Myo1D^{EY}$ ($Myo1D^{Ey08859}$) mutants with wt and mutant *Myo1D* transgenes. The key to each genotype is numbered and listed on the right.

(**D-I**) DHE labeling as ROS marker of eye imaginal discs of indicated genotype. *Myo1C* suppresses *Myo1D*-induced ROS generation (I). Scale bar: 50μm.

(**J,K**) Quantification of the DHE labelings in (D-F) and (G-I). DHE signal intensity was determined across the entire discs.

(**L-T**) NimC labeling for visualization of hemocytes attached to eye imaginal discs of indicated genotype. Note that the activated hemocyte morphology in (L,O,Q) is absent in (M,N,P,R,S,T,U). Quantifications in (V) and (W). Scale bars: 20μm.

(**V,W**) Quantification of the NimC labelings in (L-P) and (Q-U) reveals that hemocytes recruitment to undead tissue requires the IQ (neck) and tail domains of Myo1D and can be antagonized by Myo1C. NimC signal intensity was determined across the entire discs.

Figure 3. Genetic and physical interaction between Myo1D and Dronc.

(**A-D**) Head capsule phenotypes of the indicated genotypes. Scale bar: 200μm.

(**E**) Extracts from *ey>hid,p35,GFP* and *ey>hid,p35;Myo1D-GFP* eye/antennal imaginal discs were immunoprecipated with anti-GFP antibodies. Shown are immunoblots of Myo1D-

GFP immunoprecipitates probed with anti-Dronc (SK11) (top) and anti-GFP antibodies (bottom). Arrows indicate Myo1D-GFP and Dronc.

(**F**) Extracts from *ey-Gal4* (-), *ey>Flag-Dronc* and *ey>Flag-Dronc,Myo1D-HA* eye/antennal imaginal discs were immunoprecitated with anti-Flag antibodies. Shown are immunoblots probed with anti-HA antibodies to visualize Myo1D-HA (top, arrow) and with anti-Flag antibodies to reveal Flag-Dronc (bottom).

(**G**) Autoradiographs of *in vitro* cleavage assays of radio-labeled DrICE (positive control) and radio-labeled Myo1D by unlabeled active Dronc. Asterisks mark the cleavage products of DrICE.

(**H**) Immunoblot analysis of total extracts from *ey>hid,p35;Myo1D-GFP* eye/antennal imaginal discs using anti-GFP antibodies.

Figure 4. Myo1D localizes Dronc to the basal side of the plasmamembrane.

(**A**) Left: surface view of the larval eye-antennal imaginal disc at the disc proper (DP) level. Right: orthogonal section through the red square along the red dotted line. The peripodial membrane (PM; orange) and the DP (green) are separated by a lumen. The apical and basal membranes of the DP are indicated by arrows. Hemocytes approach the disc at the DP side. A-anterior; P-posterior; D-dorsal; V-ventral.

(**B-E’’’**) Confocal sections as indicated in the schematic drawing in (A) of eye imaginal discs of the indicated genotype labeled for endogenous Myo1D (green), Dronc (red) and Dlg (magenta). The discs were processed in parallel and imagined under the same settings. The peripodial membrane (PM) and the basal side of the disc proper (DP) are indicated by arrows in the sections. Scale bar: 5 μm.

(**F**) Quantification of the Dronc labelings in (B-E) at the basal side of the plasmamembrane of DP cells. Signal intensity was determined only at the basal side of the plasmamembrane.

(**G**) Immunoblot analysis of total extracts from larval eye imaginal discs of the indicated genotype suggests that endogenous Dronc protein is destabilized by absence of Myo1D due to *Myo1D* RNAi (BL33971).

(**H**) Schematic drawings of the morphology of salivary glands in surface view (top) and in sections through the middle of the gland (bottom). The basal sides of the plasmamembrane are identified by arrows. The apical sides face the lumen of the gland. Nuclei are in blue. The red square depicts the view in panels (I-L).

(**I-L’’’**) Confocal section views as illustrated by the red square in (H) of larval salivary glands of indicated genotypes labeled for endogenous Myo1D (green), Dronc (red), Dlg (magenta) and DAPI (blue). The basal sides of the plasmamembrane and the lumen are indicated by arrows. The glands were processed in parallel and imagined under the same settings. Scale bar: 50 μm.

(**M-O’**) Confocal sections according to (A) through eye imaginal discs of the indicated genotypes labeled for HA (to detect Myo1D-HA) and endogenous Dronc. Peripodial membrane (PM) and basal side of disc proper (DP) are indicated by arrows.

(**P**) Quantification of the Dronc labelings in (M’-O’) at the basal side of the plasmamembrane of DP cells. Signal intensity was determined only at the basal side of the plasmamembrane.

Figure 5. Non-apoptotic activity of Dronc at the plasmamembrane.

(**A-C’’’’**) Surface (A-A’’,B-B’’,C-C’’) and section views (A’’’,A’’’’,B’’’,**B’’’’,C’’’,C’’’’)** according to Figure 4A of eye imaginal discs of indicated genotype labeled with cleaved caspase3 (CC3, red), the polarity marker Dlg (in A; green) and endogenous Myo1D (in B,C; green). Peripodial membrane (PM) and the basal side of the disc proper (DP) are indicated by arrows on the right of the sections. In (A), apoptosis was induced by shifting to 30°C for 12 hours prior to dissection (Fan et al., 2014). Scale bar: 10μm.

(**D-E’’’**) Surface (D-D’’;E-E’’) and section views (D’’’;E’’’) of larval salivary glands (SG) according to Figure 4H of the indicated genotype labeled with CC3 and the polarity marker Dlg. In the sections, the basal sides of the plasmamembrane and the lumen are indicated by arrows.

(**F,G**) Surface views of larval SGs of indicated genotype labeled for CC3 (green), the polarity marker Dlg (red) and DAPI (blue). Normal SGs have weak membrane localization of CC3 (F') that is completely lost upon *Myo1D* RNAi driven by *Fkh-Gal4* (G'). Scale bar: 20μm.

(**H**) Illustration of the specificities of CC3 and cDcp1 antibodies with respect to the apoptotic and non-apoptotic cleavage targets of Dronc.

(**I,K'**) $dronc^{I24/I24}$ (I) mutant and $dcp^{Prev/Prev}$;$drICE^{\Delta 1/\Delta 1}$ (J,K) double mutant SGs labeled for CC3 in (I,K), cleaved Dcp1 (cDcp1) in (J), the polarity marker Dlg and DAPI. Scale bars: 20μm.

Figure 6. Myo1D requires Duox for its function in apoptosis-induced proliferation.

(**A-C**) The overgrown head capsule (A) of *ey>p35,Myo1D-GFP* animals correlates with ROS production (DHE labeling in (B)) and activated hemocytes (NimC labeling in (C)) in larval imaginal eye discs. Scale bars: 200, 50 and 20 μm in (A), (B) and (C), respectively.

(**D-F**) Knockdown of *Duox* in *ey>p35,Myo1D-GFP* animals suppresses the overgrowth of the head capsule (D), ROS production (E) and hemocytes activation (F).

(**G,H**) Quantification of DHE (G) and NimC (H) labelings in (B,E) and (C,F) panels, respectively. Signal intensities were determined across entire discs.

(**I-K**) Endogenous Duox (magenta) and Dronc (red) proteins co-localize at the PM and basal plasmamembrane of DP cells in *ey>hid,p35* eye imaginal discs. Scale bar: 10 μm.

(**L-N**) Endogenous Duox (magenta) and Dronc (red) proteins co-localize at the basal side of the plasmamembrane of larval *ey>hid,p35* SG cells. Blue = DAPI (nuclei). Scale bar: 20 μm.

(**O-R**) Myo1D and Duox synergize for production of ROS in *ey>p35* discs. Scale bar: 50 μm.

(**S**) Quantification of DHE labelings in (O-R). Signal intensities were determined across entire discs. ns - not significant.

(**T,U**) *dronc* RNAi suppresses overgrowth of head capsules of (T) and ROS generation in eye discs (U) of *ey>p35,Myo1D-GFP* animals (compare to A,B).

Figure 7. *Myo1D* is required for neoplastic tumor growth and invasion of *scrib*$^{-/-}$*Ras*^{V12} cells.

scrib$^{-/-}$*Ras*^{V12} mutant clones are generated by the MARCM system and are marked by GFP. *UAS-lacZ* was used as control transgene in (A,D,G,J).

(**A-L**) Growth of *scrib*$^{-/-}$*Ras*^{V12} clones (A), invasion of mutant tissue into the ventral nerve cord (VNC) of the larval brain (D, arrow), generation of ROS (DHE) by *scrib*$^{-/-}$*Ras*^{V12} mosaic discs (G) and recruitment and activation (arrows in J) of hemocytes (NimC) to *scrib*$^{-/-}$*Ras*^{V12} mosaic discs (J) is prevented by *Myo1D* RNAi (BL33791) (B,E,H,K). OL – optic lobe. Quantifications in (C,F,I,L). Signal intensities (GFP, DHE, NimC) were determined across entire discs. Scale bars: 50 μm in A,B,G,H,J,K; 100 μm (D,E).

(**M-N'**) Membrane association of Dronc protein in *scrib*$^{-/-}$*Ras*^{V12} mutant clones (M') is disrupted by *Myo1D* RNAi (N'). Scale bars: 20 μm.

Figure 8. Model of Myo1D function in apoptosis-induced proliferation

The data presented in this paper suggest that Myo1D is required for membrane localization of Dronc, specifically to the basal side of the plasmamembrane of undead epithelial disc proper and salivary gland cells. Here, Dronc is required for activation of Duox for generation of extracellular ROS. Duox-generated ROS attract and activate hemocytes to the basal side of disc proper cells of eye imaginal discs. Hemocytes release Eiger to stimulate JNK activity and AiP in undead epithelial cells.

STAR METHODS

Contact for reagent and resource sharing

Please contact Andreas Bergmann (andreas.bergmann@umassmed.edu)

Method Details

Genetics and fly stocks

To test mutants or RNAi lines for involvement in AiP, they were crossed to the *ey>hid,p35* stock (exact genotype: *UAS-hid; ey-Gal4 UAS-p35*/*CyO,tub-Gal80* (Fan et al., 2014) and the offspring was scored for suppression of head capsule overgrowth. Unless otherwise noted, the *ey>p35* (*ey-Gal4 UAS-p35*/*CyO*) was used in control crosses. Most crosses were performed with the *UAS*/*Gal4* system (Brand and Perrimon, 1993). $scrib^{-/-}$ Ras^{V12} clones were induced using the MARCM technique (Lee and Luo, 1999). The $scrib^{2}$ allele was used.
$Myo1D^{K2}$ (a kind gift of S. Noselli (Nice, France)) was obtained by imprecise excision of a P-allele of *Myo1D*, $Myo1D^{KG02246}$, and deletes almost the entire *Myo1D* locus (Speder et al., 2006). $Myo1D^{Ey08859}$ (BL19940) carries a P-element insertion one nucleotide after the transcriptional start side. All other stocks are listed in the Key Resources Table

Immunolabeling and DHE stainings

For labeling with antibodies, fixed eye/antennal imaginal discs were used following standard protocols (Fan and Bergmann, 2014; Fogarty and Bergmann, 2014). The anti-Myo1D antibody (1:200; Abmart, Shanghai,China) is a monoclonal antibody raised against the F^{526}KRLLHNSKDAN epitope in the head domain of Myo1D. Fluorescent secondary antibodies were obtained from Jackson ImmunoResearch. DHE labelings were performed on unfixed imaginal discs as described previously (Owusu-Ansah et al., 2008).

Co-immunoprecipation (co-IP) and immunoblotting

Figure 3E: Because the available Myo1D antibody did not perform in IP experiments, *UAS-Myo1D-GFP* was crossed into *ey>hid,p35* background and IP experiments were performed with GFP-Trap_M beads (15µl, Chromotek) from larval extracts. Immunoprecipitates were separated on 4-15% gradient SDS-PAGE and blotted on PVDF membranes. GFP (1:1000; Pierce) and Dronc (SK11) (1:1000; gift of P. Meier) antibodies were used for immunoblotting. For the reverse experiment (Figure 3F), *Flag-Dronc* and *Myo1D-HA* were crossed into *ey-Gal4* background and immunoprecipitates using anti-Flag M2 magnetic beads (35µl, Sigma-Aldrich) were separated by SDS-PAGE. Immunoblots were probed with HA (1:1000; Pierce) and Flag (1:1000, Sigma-Aldrich) antibodies. For Figure 3H, total extracts of *ey>hid,p35,Myo1D-GFP* and *ey>hid,p35,Myo1D-GFP,Flag-Dronc* imaginal discs were analyzed by immunoblotting with GFP antibodies.

In vitro Dronc cleavage assays

To test if Dronc can proteolytically process Myo1D *in vitro*, recombinant 6x-His-Dronc protein in pET23b (gift of G. Salvesen) was expressed in *E.coli* strain BL21pLysS(DE3) and purified using published protocols (Dorstyn and Kumar, 2008; Kamber Kaya et al., 2017; Snipas et al., 2008). A significant fraction of Dronc protein undergoes autocleavage and is proteolytically active within 24h after preparation. Myo1D and the positive control $DrICEC^{211A}$ (which is a

catalytic mutant to avoid autoprocessing) were cloned into pBluescript and synthesized *in vitro* as S^{35}-labeled proteins in rabbit reticulocyte lysates (Promega) with T7 polymerase. These radiolabeled proteins were incubated with the active Dronc preparations for 90 min at 25°C and separated by SDS-Page. Gels were dried and exposed to autoradiography overnight.

Quantification and statistics.

For quantification of confocal images, the 'Record Measurement' function of Photoshop was used. Discs were outlined and signal intensity determined. Crosses were repeated at least three times. Analysis and graph generation was done using GraphPad Prism 7.03. The statistical method used was the student's T-test, one-tailored distribution, two sample unequal variance, unless otherwise indicated. Plotted is mean intensity ± SE. P values: ** P<0.01; *** P<0.001; **** P <0.0001.

N numbers are as follows:

Figure 1P: n = 4, 15, and 8 for control, *ey>hid,p35* and *ey>hid, p35;Myo1D^{RNAi}*, respectively.

Figure 1T: n = 6, 9 and 6 for control, *ey>hid,p35* and *ey>hid, p35;Myo1D^{RNAi}*, respectively.

Figure 2J: n = 5, 5 and 7 (D-F).

Figure 2K: n = 4, 6 and 6 (G-I).

Figure 2V: n = 19, 5, 8, 7, 7 (K-O)

Figure 2W: n = 15, 6, 6, 4, 4 (P-T).

Figure 4F: n = 10, 6, 10, 4 (B-E).

Figure 4P: n = 5, 4, 6 (N-O).

Figure 6G: n = 4, 8, 4 for *ey>p35*; *ey>p35,Myo1D*; *ey>p35, Myo1D, Duox ^{RNAi}*, respectively.

Figure 6H: n = 3, 9, 4 for *ey>p35*; *ey>p35,Myo1D*; *ey>p35, Myo1D, Duox ^{RNAi}*, respectively.

Figure 6S: n = 4, 5, 5, 4 for *ey>p35, ey>p35,Myo1D, ey>p35,Duox, ey>p35,Myo1D+Duox*, respectively.

Figure 7C: n = 9 and 7 for *scrib$^{-/-}$Ras^{V12}* and *scrib$^{-/-}$Ras^{V12},Myo1D^{RNAi}*.

Figure 7F: n = 5 and 5 for *scrib$^{-/-}$Ras^{V12}* and *scrib$^{-/-}$Ras^{V12},Myo1D^{RNAi}*.

Figure 7I: n = 3 and 4 for *scrib$^{-/-}$Ras^{V12}* and *scrib$^{-/-}$Ras^{V12},Myo1D^{RNAi}*.

Figure 7L: n = 5 and 3 for *scrib$^{-/-}$Ras^{V12}* and *scrib$^{-/-}$Ras^{V12},Myo1D^{RNAi}*.

KEY RESOURCES TABLE

REAGENT or RESOURCE	SOURCE	IDENTIFIER
Antibodies		
Mouse monoclonal NimC (1:300)	Kindly provided by I. Ando	(Kurucz et al., 2007)
Guinea pig Dronc (1:200)	Kindly provided by P. Meier	SK11; (Wilson et al., 2002)
Rabbit polyclonal Cleaved Caspase 3 (CC3) (1:400)	Cell Signaling Technology	Cat#9661S
Mouse monoclonal Wg (1:50)	DSHB	Cat#4D4
Mouse monoclonal Myo1D (1:250)	Abmart, Shanghai,China	Cat#20735-1-16/P23_141121
Rabbit polyclonal Duox (1:100)	LS Bio	Cat#C410118
Rabbit polyclonal Cleaved Dcp1 (cDCP1) (1:200)	Cell Signaling Technology	Cat#9578S
Mouse monoclonal β-Gal (1:100)	Promega	Cat#Z378A
Rabbit polyclonal Phospho-JNK (pJNK) (1:200)	Promega	Cat#V793B
Mouse monoclonal GFP (Western Blot-1:1000)	Pierce	Cat#MA15256
Rat polyclonal ELAV (1:50)	DSHB	Cat#7EBA10
Mouse monoclonal HA (1:200, Western Blot-1:2000)	Invitrogen	Cat#26183
Mouse monoclonal FLAG (Western Blot-1:1000)	Sigma-Aldrich	Cat#F1804
Bacterial and Virus Strains		
E.coli strain BL21pLysS(DE3)	Promega	Cat#L1191
Chemicals, Peptides, and Recombinant Proteins		
DHE	Invitrogen	Cat#D23107
Gfp-Trap_M beads	Chromotek	Cat#Gtm-20
anti-Flag M2 magnetic beads	Sigma-Aldrich	Cat#M8823
6x-His-Dronc protein	Kindly provided by G.Salvesen	(Snipas et al., 2008)
DrICEC^{211A}	Kindly provided by G.Salvesen	(Snipas et al., 2008)
Vectashield with DAPI	Vector Laboratories	Cat#H-1200
Critical Commercial Assays		
Rabbit reticulocyte lysates	Promega	Cat#L4610
In Situ Cell Death Detection Kit, TMR red	Roche	Cat#12156792910
Experimental Models: Organisms/Strains		
UAS-hid; ey-Gal4 UAS-p35/CyO,tub-Gal80		(Fan et al., 2014)
ey-Gal4 UAS-p35/CyO		(Fan et al., 2014)
scrib$^{-/-}$ Ras^{V12}	Kindly provided by M. Kango-Singh	(Chen et al., 2012)
Myo1D RNAi	Bloomington Drosophila Stock Center	BDSC33971 FlyBase: FBst0033971
Myo1D RNAi	Vienna Drosophila RNAi Center	v102456 FlyBase:FBst0475947
Myo1D^{K2}	Kindly provided by S. Noseli	FlyBase:FBal0194493 (Speder et al., 2006)
Myo1D^{Ey08859}	Bloomington Drosophila Stock Center	FlyBase:FBst0019940
UAS-Myo1D	Kindly provided by S. Noseli	(Speder et al., 2006)
UAS-Myo1D-GFP	Kindly provided by S. Noseli	(Speder et al., 2006)

UAS-Myo1D-HA	Kindly provided by K. Matsun,	FlyBase:FBtp0081821 (Hozumi et al., 2008)
UAS-Myo1C-HA	Kindly provided by K. Matsuno	(Hozumi et al., 2008)
UAS-Myo1D/1C-HA	Kindly provided by K. Matsuno	FlyBase:FBtp0081835 (Hozumi et al., 2008)
UAS-Myo1C/1D-HA	Kindly provided by K. Matsuno	(Hozumi et al., 2008)
UAS-Myo1D-HA^{mATP}	Kindly provided by K. Matsuno	FlyBase:FBtp0081822 (Hozumi et al., 2008)
UAS-Myo1D-HA$^{\Delta Abs}$	Kindly provided by K. Matsuno	FlyBase:FBtp0081824 (Hozumi et al., 2008)
UAS-Myo1D-HA$^{\Delta IQ}$	Kindly provided by K. Matsuno	FlyBase:FBtp0081825 (Hozumi et al., 2008)
UAS-Myo1D-HA$^{\Delta tail}$	Kindly provided by K. Matsuno	FlyBase:FBtp0081826 (Hozumi et al., 2008)
UAS-Flag-dronc	Bergmann lab	FlyBase:FBtp0093662 (Kamber Kaya et al., 2017)
UAS-dark-GFP	Kindly provided by H-D Ryoo	FlyBase:FBtp0116994 (Shapiro et al., 2008)
UAS-dronc RNAi	Kindly provided by P. Meier	BDSC32963 FlyBase:FBst0032963 (Leulier et al., 2006)
UAS-Duox RNAi	Kindly provided by W. J. Lee	FlyBase:FBal0190061 (Ha et al., 2005)
UAS-Duox	Kindly provided by W. J. Lee	FlyBase:FBal0190278 (Ha et al., 2005)
dronc^{I24}	Bergmann lab	FlyBase:FBal0190335 (Xu et al., 2005)
dcp1^{Prev}	Kindly provided by K. McCall	FlyBase:FBal0156746 (Laundrie et al., 2003)
drICE$^{\Delta 1}$	Kindly provided by B. Hay	FlyBase:FBal0193685 (Muro et al., 2006)
DE-Gal4	Kindly provided by G. Halder	(Morrison and Halder, 2010)
UAS-hid/+; DE-Gal4 tub-Gal80^{ts}/+	Bergmann lab	(Fan et al., 2014)
Nub-Gal4		(Calleja et al., 1996)
GMR-Gal4 UAS-eiger	Kindly provided by M. Miura	(Igaki et al., 2002)
UAS-bsk RNAi	Vienna Drosophila RNAi Center	v34138 FlyBase:FBst0460476
UAS-Traf2 RNAi	Vienna Drosophila RNAi Center	v110266 FlyBase:FBst0481844
puc-lacZ		FlyBase:FBal0047865 (Ring and Martinez Arias, 1993)
GMR-hid	Kindly provided by H. Steller	FlyBase:FBal0265023 (Grether et al., 1995)
UAS-Empty Vector (UAS-EV)	Bergmann lab	(Kamber Kaya et al., 2017)
Canton S		FlyBase:FBst0064349
w1118		FlyBase:FBst0003605

w; Kr^{If-1}/CyO; M{lexAop-UAS-GrabFP.A.Int.mCh}ZH-86Fb/TM6B, Tb^{1}*	Bloomington Drosophila Stock Center	FlyBase:FBst0068178 (Harmansa et al., 2017)

Detailed Genotypes

Figure	Panel	Genotype
1	B, M,M',Q,V	*+/+;ey>p35/+;+/+*
	C,N,N',R	*UAS-hid/+;ey>p35/+;+/+*
	D	*UAS-hid/+;ey>p35/UAS-Empty Vector (EV);+/+*
	E	*UAS-hid/+;ey>p35/UAS-Myo1D RNAi;+/+*
	F,O,O',S	*UAS-hid/+;ey>p35/+;UAS-Myo1D RNAi/+*
	G	*UAS-hid/+;ey>p35/Myo1D^{K2};+/+*
	H	*UAS-hid/+;ey>p35/Myo1D^{Ey08859};+/+*
	I	*UAS-hid/+;ey>p35/+;UAS-Myo1D/+*
	J,J'	*+/+;ey>p35/+;puc-lacZ/+*
	K,K'	*UAS-hid/+;ey>p35/+;puc-lacZ/+*
	L,L'	*UAS-hid/+;ey>p35/UAS-Myo1D RNAi; puc-lacZ/+*
	W	*+/+;ey>p35/+;UAS-Myo1D/+*
2	D,L	*UAS-hid/+;ey>p35/+;+/+*
	E,M	*UAS-hid/+;ey>p35/+;UAS-Myo1D$^{\Delta IQ}$-HA/+*
	F,N	*UAS-hid/+;ey>p35/UAS-Myo1C-HA;+/+*
	G,Q	*+/+;ey>p35/+;UAS-Myo1D-HA/+*
	H,R	*+/+;ey>p35/+;UAS-Myo1D$^{\Delta IQ}$-HA/+*
	I,U	*+/+;ey>p35/UAS-Myo1C-HA;UAS-Myo1D-HA/+*
	O	*UAS-hid/+;ey>p35/+;UAS- Myo1C^{H} -Myo1D$^{IQ\text{-}tail}$-HA/+*
	P	*UAS-hid/+;ey>p35/+; UAS- Myo1D^{H} -Myo1C$^{IQ\text{-}tail}$-HA /+*
	S	*+/+;ey>p35/+;UAS-Myo1D$^{\Delta tail}$-HA/+*
	T	*+/+;ey>p35/UAS-Myo1C-HA;+/+*
3	A	*+/+;ey>p35/+;+/+*
	B	*+/+;ey>p35/UAS-Flag-Dronc;+/+*
	C	*+/+; ey>p35/+;UAS-Myo1D-HA/+*
	D	*+/+; ey>p35/UAS-Flag-Dronc;UAS-Myo1D-HA/+*
	E	lane 1: *UAS-hid/+;ey>p35/+;UAS-GFP/+* lane 2: *UAS-hid/+;ey>p35/+;UAS-Myo1D-GFP/+*
	F	lane 1: *+/+;ey-Gal4/+;+/+* lane 2: *+/+;ey-Gal4/UAS-Flag-dronc;+/+* lane 3: *+/+;ey-Gal4/UAS-Flag-dronc;UAS-Myo1D-HA/+*
	H	lane 1: *UAS-hid/+;ey>p35/+; UAS-Myo1D-GFP/+* lane 2: *UAS-hid/+;ey>p35/UAS-Flag-dronc; UAS-Myo1D-GFP/+*
4	B-B'',I-I'''	*+/+;ey-Gal4/+;+/+*
	C-C'',J-J'''	*+/+;ey-Gal4/+;UAS-Myo1D RNAi/+*
	D-D'',K-K'''	*UAS-hid/+;ey>p35/+;+/+*
	E-E'',L-L'''	*UAS-hid/+;ey>p35/+; UAS-Myo1D RNAi /+*
	G	lane 1: *UAS-hid/+;ey>p35/UAS-Flag-Dronc;+/+* lane 2: *UAS-hid/+;ey>p35/UAS-Flag-Dronc;UAS-Myo1D RNAi/+*
	M-M'	*UAS-hid/+;ey>p35/+; UAS-Myo1D-HA /+*

	N-N’	*UAS-hid/+;ey>p35/+;UAS-Myo1D$^{\Delta IQ}$-HA/+*
	O-O’	*UAS-hid/+;ey>p35/+;UAS-Myo1D$^{\Delta tail}$-HA/+*
5	A-A’’’’	*UAS-hid/+;UAS-GFP/+;DE-Gal4 TubulinGal80^{ts}/+*
	B-B’’’’,D-D’’’’	*UAS-hid/+;ey>p35/+;+/+*
	C-C’’’’,E-E’’’’	*UAS-hid/+;ey>p35/+; UAS-Myo1D RNAi /+*
	F-F’	*+/+;Fkh-Gal4/+;+/+*
	G-G’	*+/+;Fkh-Gal4/+; UAS-Myo1D RNAi*
	H-H’	*+/+;+/+;dronc^{I24}/Dronc^{I24}*
	J-K’	*+/+;dcp1^{Prev}/dcp1^{Prev};drice$^{\Delta 1}$/drice$^{\Delta 1}$*
6	A-C	*+/+;ey>p35/+;UAS-Myo1D-GFP/+*
	D-F	*+/+;ey>p35/UAS-Duox RNAi;UAS-Myo1D-GFP/+*
	I-N	*UAS-hid/+;ey>p35/+;+/+*
	O	*+/+;ey>p35/+;+/+*
	P	*+/+;ey>p35/UAS-Duox;+/+*
	Q	*+/+;ey>p35/+;UAS-Myo1D-HA/+*
	R	*+/+;ey>p35/UAS-Duox;UAS-Myo1D-HA/+*
	T,U	*+/+;ey>p35/UAS-DroncRNAi;UAS-Myo1D-GFP/+*
7	A-J,M,M’	*ey-FLP/+; act>y+>Gal4, UAS-GFP56ST/UAS-LacZ; FRT82B tub-Gal80/UAS-RasV12 FRT82B scrib2*
	B-K,N,N’	*ey-FLP/+; act>y+>Gal4, UAS-GFP56ST/UAS-Myo1D RNAi; FRT82B tub-Gal80/UAS-RasV12 FRT82B scrib2*
S1	A	*+/+;ey-Gal4/+;+/+*
	B-D	*UAS-hid/+;ey>p35/+;+/+*
	E,E’	*+/+;GMR-hid/+;DE-Gal4>UAS-GFP/+*
	F,F’	*+/+;GMR-hid/UAS-Myo1D RNAi;DE-Gal4>UAS-GFP/+*
	G,G’	*UAS-hid/+;Nub-Gal4/+;+/+*
	H,H’	*UAS-hid/+;Nub-Gal4/+; UAS-Myo1D RNAi /+*
	I-I’’	*UAS-hid/+;Nub-Gal4/+; UAS-p35/+*
	J-J’	*UAS-hid/+;ey>p35/+;+/+*
	K-K’	*UAS-hid/+;ey>p35/UAS-Myo1D RNAi;+/+*
S2	B	*+/+;GMR-Gal4>UAS-eiger/+;+/+*
	C	*+/+;GMR-Gal4>UAS-eiger/Traf2 RNAi;+/+*
	D	*+/+;GMR-Gal4>UAS-eiger/Bsk RNAi;+/+*
	E	*+/+;GMR-Gal4>UAS-Eiger/Myo1D RNAi;+/+*
S3	A,A’,C,C’	*+/+;ey>p35/+;+/+*
	B,B’,D,D’	*+/+;ey>p35/+;UAS-Myo1D/+*
S4	A	*UAS-hid/+;ey>p35/+;+/+*
	B	*UAS-hid/+;ey>p35/+;UAS-Myo1D$^{\Delta IQ}$-HA/+*
	C	*UAS-hid/+;ey>p35/+;UAS-Myo1D$^{\Delta tail}$-HA/+*
	D	*UAS-hid/+;ey>p35/UAS-Myo1C-HA;+/+*

	E	*UAS-hid/+;ey>p35/+;UAS- Myo1C^{H} -Myo1D$^{IQ\text{-}tail}$-HA/+*
	F	*UAS-hid/+;ey>p35/+; UAS- Myo1D^{H} -Myo1C$^{IQ\text{-}tail}$-HA /+*
	G	*+/+;ey>p35/+;+/+*
	H	*+/+;ey>p35/+;UAS-Myo1D/+*
	I	*UAS-hid/+;ey>p35/+;UAS-Myo1D$^{\Delta IQ}$-HA/+*
	J	*UAS-hid/+;ey>p35/+;UAS-Myo1D$^{\Delta tail}$-HA/+*
S5	A-A''	*UAS-hid/+;ey>p35/+;UAS-Myo1D-GFP/+*
	B-B'''	*UAS-hid/+;ey>p35/CyO;UAS-Myo1D-GFP/ UAS-GrabFP.A.Int.mCh}ZH-86Fb*
S6	A	*+/+;ey-Gal4/UAS-Dark-GFP;+/+*
	B,D-D''	*UAS-hid/+;ey>p35/UAS-Dark-GFP;+/+*
	C	*UAS-hid/+;ey>p35/UAS-Dark-GFP;UAS-Myo1D RNAi/+*

Brand, A.H., and Perrimon, N. (1993). Targeted gene expression as a means of altering cell fates and generating dominant phenotypes. Development *118*, 401-415.

Calleja, M., Moreno, E., Pelaz, S., and Morata, G. (1996). Visualization of gene expression in living adult Drosophila. Science *274*, 252-255.

Chen, C.L., Schroeder, M.C., Kango-Singh, M., Tao, C., and Halder, G. (2012). Tumor suppression by cell competition through regulation of the Hippo pathway. Proceedings of the National Academy of Sciences of the United States of America *109*, 484-489.

Dorstyn, L., and Kumar, S. (2008). A biochemical analysis of the activation of the Drosophila caspase DRONC. Cell Death Differ *15*, 461-470.

Fan, Y., and Bergmann, A. (2014). Multiple mechanisms modulate distinct cellular susceptibilities toward apoptosis in the developing Drosophila eye. Developmental cell *30*, 48-60.

Fan, Y., Wang, S., Hernandez, J., Yenigun, V.B., Hertlein, G., Fogarty, C.E., Lindblad, J.L., and Bergmann, A. (2014). Genetic models of apoptosis-induced proliferation decipher activation of JNK and identify a requirement of EGFR signaling for tissue regenerative responses in Drosophila. PLoS Genet *10*, e1004131.

Fogarty, C.E., and Bergmann, A. (2014). Detecting caspase activity in Drosophila larval imaginal discs. Methods Mol Biol *1133*, 109-117.

Grether, M.E., Abrams, J.M., Agapite, J., White, K., and Steller, H. (1995). The head involution defective gene of Drosophila melanogaster functions in programmed cell death. Genes Dev *9*, 1694-1708.

Ha, E.M., Oh, C.T., Bae, Y.S., and Lee, W.J. (2005). A direct role for dual oxidase in Drosophila gut immunity. Science *310*, 847-850.

Harmansa, S., Alborelli, I., Bieli, D., Caussinus, E., and Affolter, M. (2017). A nanobody-based toolset to investigate the role of protein localization and dispersal in Drosophila. eLife *6*.

Hozumi, S., Maeda, R., Taniguchi-Kanai, M., Okumura, T., Taniguchi, K., Kawakatsu, Y., Nakazawa, N., Hatori, R., and Matsuno, K. (2008). Head region of unconventional myosin I family members is responsible for the organ-specificity of their roles in left-right polarity in Drosophila. Developmental dynamics : an official publication of the American Association of Anatomists *237*, 3528-3537.

Igaki, T., Kanda, H., Yamamoto-Goto, Y., Kanuka, H., Kuranaga, E., Aigaki, T., and Miura, M. (2002). Eiger, a TNF superfamily ligand that triggers the Drosophila JNK pathway. EMBO J *21*, 3009-3018.

Kamber Kaya, H.E., Ditzel, M., Meier, P., and Bergmann, A. (2017). An inhibitory mono-ubiquitylation of the Drosophila initiator caspase Dronc functions in both apoptotic and non-apoptotic pathways. PLoS Genet *13*, e1006438.

Kurucz, E., Vaczi, B., Markus, R., Laurinyecz, B., Vilmos, P., Zsamboki, J., Csorba, K., Gateff, E., Hultmark, D., and Ando, I. (2007). Definition of Drosophila hemocyte subsets by cell-type specific antigens. Acta biologica Hungarica *58 Suppl*, 95-111.

Laundrie, B., Peterson, J.S., Baum, J.S., Chang, J.C., Fileppo, D., Thompson, S.R., and McCall, K. (2003). Germline cell death is inhibited by P-element insertions disrupting the dcp-1/pita nested gene pair in Drosophila. Genetics *165*, 1881-1888.

Lee, T., and Luo, L. (1999). Mosaic analysis with a repressible cell marker for studies of gene function in neuronal morphogenesis. Neuron *22*, 451-461.

Leulier, F., Ribeiro, P.S., Palmer, E., Tenev, T., Takahashi, K., Robertson, D., Zachariou, A., Pichaud, F., Ueda, R., and Meier, P. (2006). Systematic in vivo RNAi analysis of putative components of the Drosophila cell death machinery. Cell Death Differ *13*, 1663-1674.

Morrison, C.M., and Halder, G. (2010). Characterization of a dorsal-eye Gal4 Line in Drosophila. Genesis *48*, 3-7.

Muro, I., Berry, D.L., Huh, J.R., Chen, C.H., Huang, H., Yoo, S.J., Guo, M., Baehrecke, E.H., and Hay, B.A. (2006). The Drosophila caspase Ice is important for many apoptotic cell deaths and for spermatid individualization, a nonapoptotic process. Development *133*, 3305-3315.

Owusu-Ansah, E., Yavari, A., and Banerjee, U. (2008). A protocol for in vivo detection of reactive oxygen species. Nature Protocol Exchange

Ring, J.M., and Martinez Arias, A. (1993). puckered, a gene involved in position-specific cell differentiation in the dorsal epidermis of the Drosophila larva. Dev Suppl, 251-259.

Shapiro, P.J., Hsu, H.H., Jung, H., Robbins, E.S., and Ryoo, H.D. (2008). Regulation of the Drosophila apoptosome through feedback inhibition. Nat Cell Biol *10*, 1440-1446.

Snipas, S.J., Drag, M., Stennicke, H.R., and Salvesen, G.S. (2008). Activation mechanism and substrate specificity of the Drosophila initiator caspase DRONC. Cell Death Differ *15*, 938-945.

Speder, P., Adam, G., and Noselli, S. (2006). Type ID unconventional myosin controls left-right asymmetry in Drosophila. Nature *440*, 803-807.

Wilson, R., Goyal, L., Ditzel, M., Zachariou, A., Baker, D.A., Agapite, J., Steller, H., and Meier, P. (2002). The DIAP1 RING finger mediates ubiquitination of Dronc and is indispensable for regulating apoptosis. Nat Cell Biol *4*, 445-450.

Xu, D., Li, Y., Arcaro, M., Lackey, M., and Bergmann, A. (2005). The CARD-carrying caspase Dronc is essential for most, but not all, developmental cell death in Drosophila. Development *132*, 2125-2134.

Figure 1

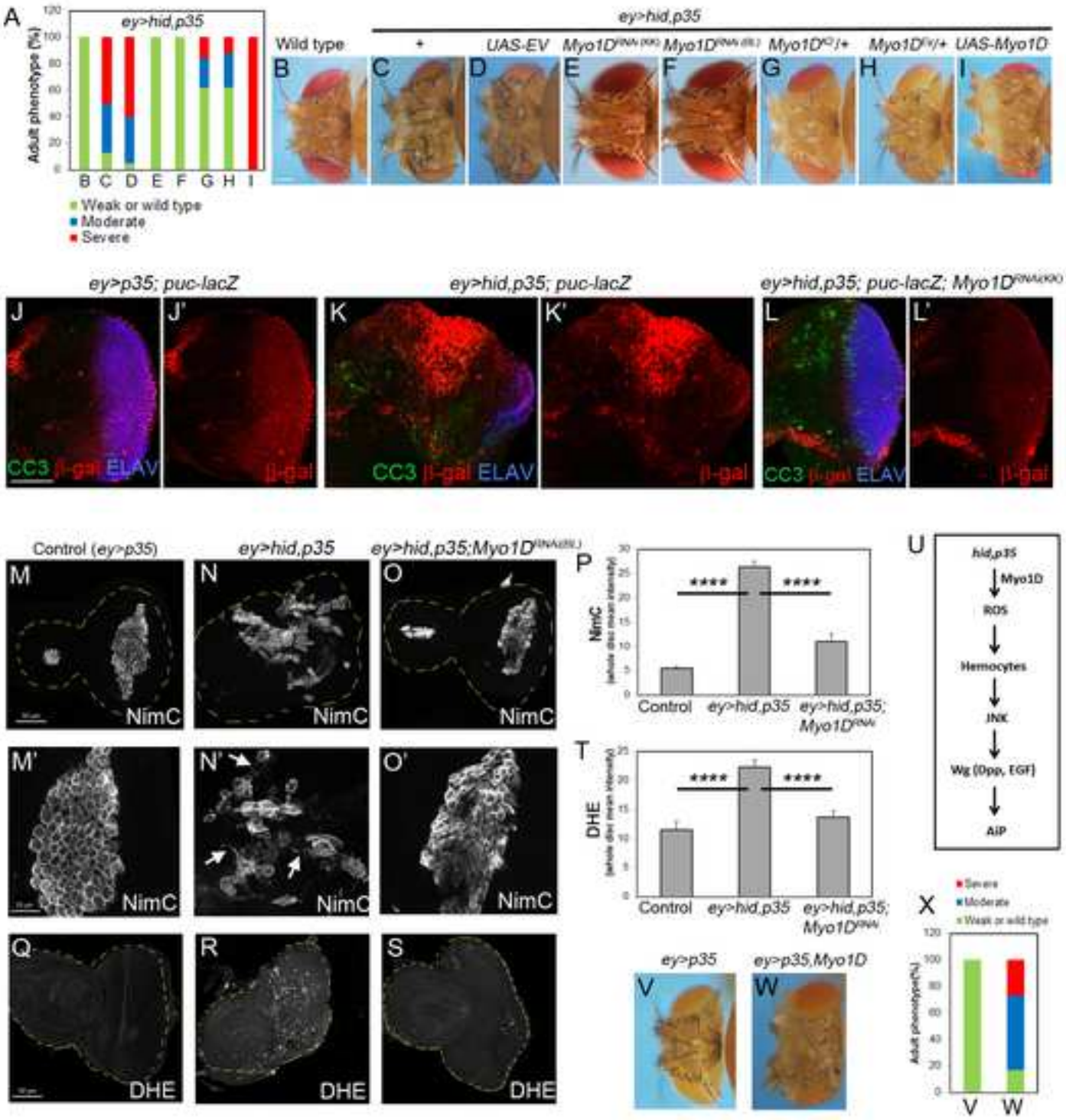
A
ey>hid,p35
Adult phenotype (%)
B C D E F G H I
Weak or wild type
Moderate
Severe
ey>hid,p35
Wild type
+
UAS-EV
Myo1D^RNA (KK)
Myo1D^RNA (BL)
Myo1D^G1/+
Myo1D^ky1/+
UAS-Myo1D
B
C
D
E
F
G
H
I
ey>p35; puc-lacZ
ey>hid,p35; puc-lacZ
ey>hid,p35; puc-lacZ; Myo1D^RNA(KK)
J
J'
K
K'
L
L'
CC3 β-gal ELAV
β-gal
Control (ey>p35)
ey>hid,p35
ey>hid,p35;Myo1D^RNA(BL)
M
N
O
M'
N'
O'
NimC
Q
R
S
DHE
P
NimC
Control
ey>hid,p35
ey>hid,p35; Myo1D^RNAi
****
T
DHE
U
hid,p35
Myo1D
ROS
Hemocytes
JNK
Wg (Dpp, EGF)
AIP
X
Severe
Moderate
Weak or wild type
Adult phenotype(%)
V W
ey>p35
ey>p35,Myo1D
V
W

Figure 2

Click here to download Figure Figure 2.tif

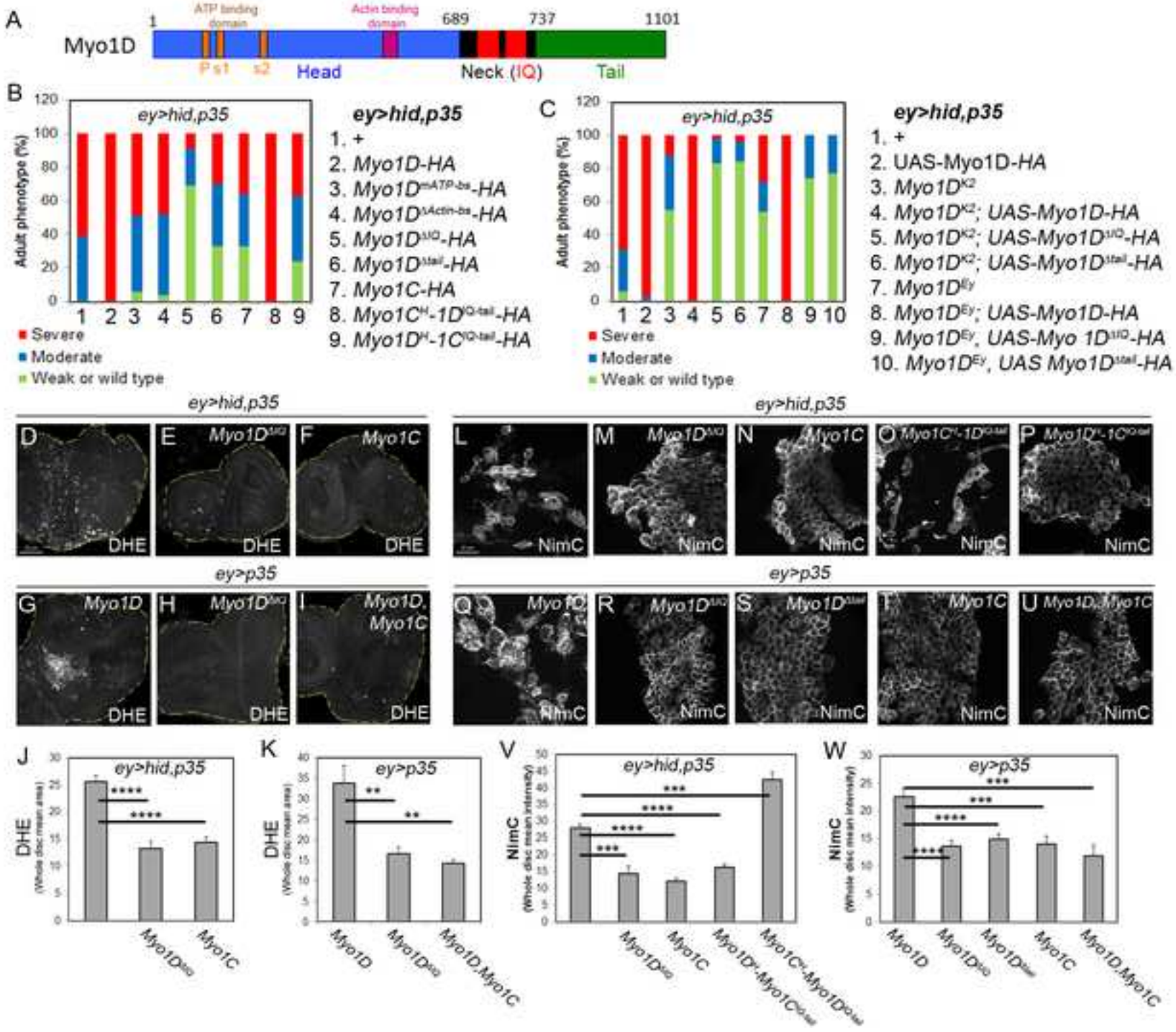

Figure 3

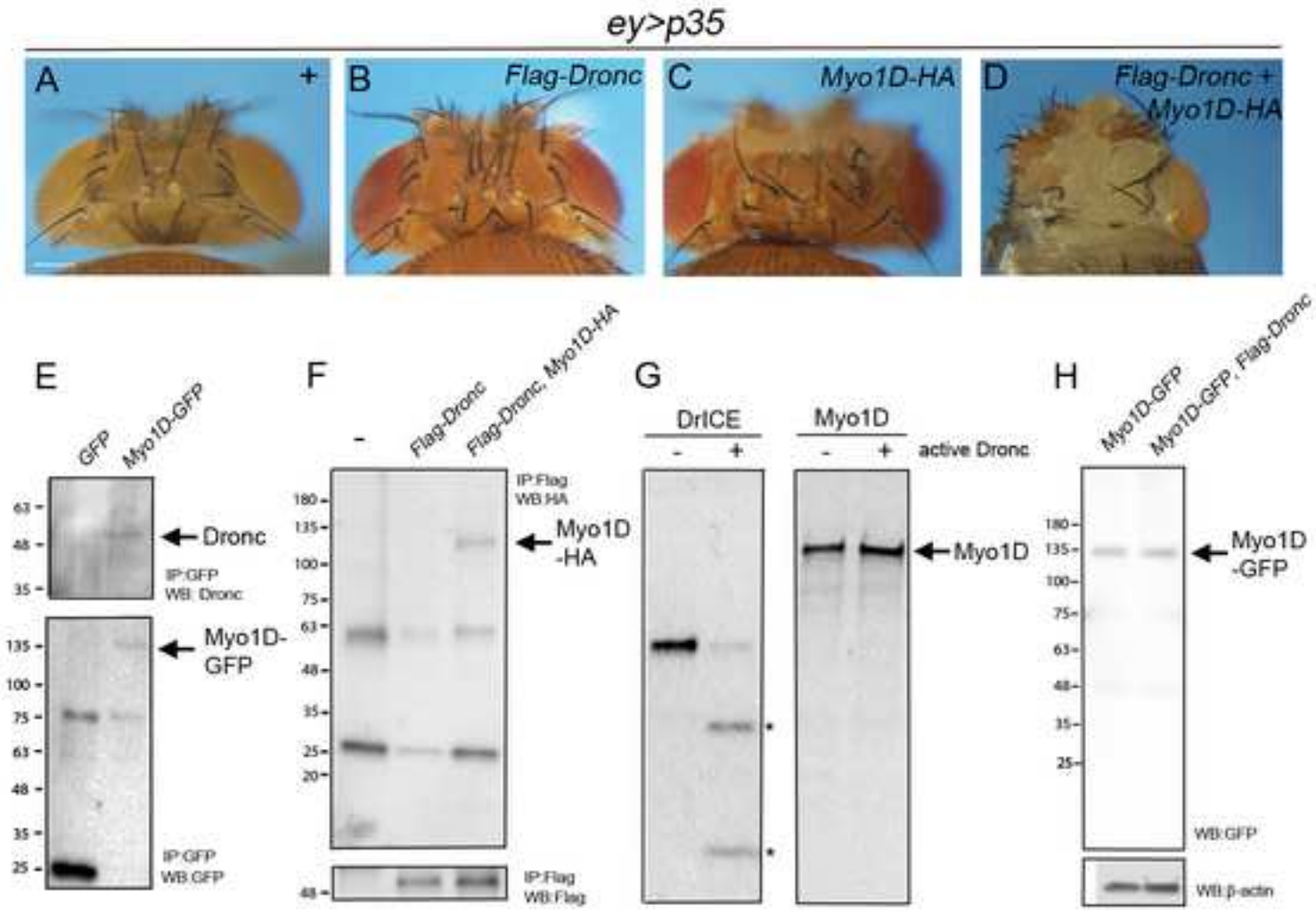

Figure 4

Click here to download Figure Figure 4.tif

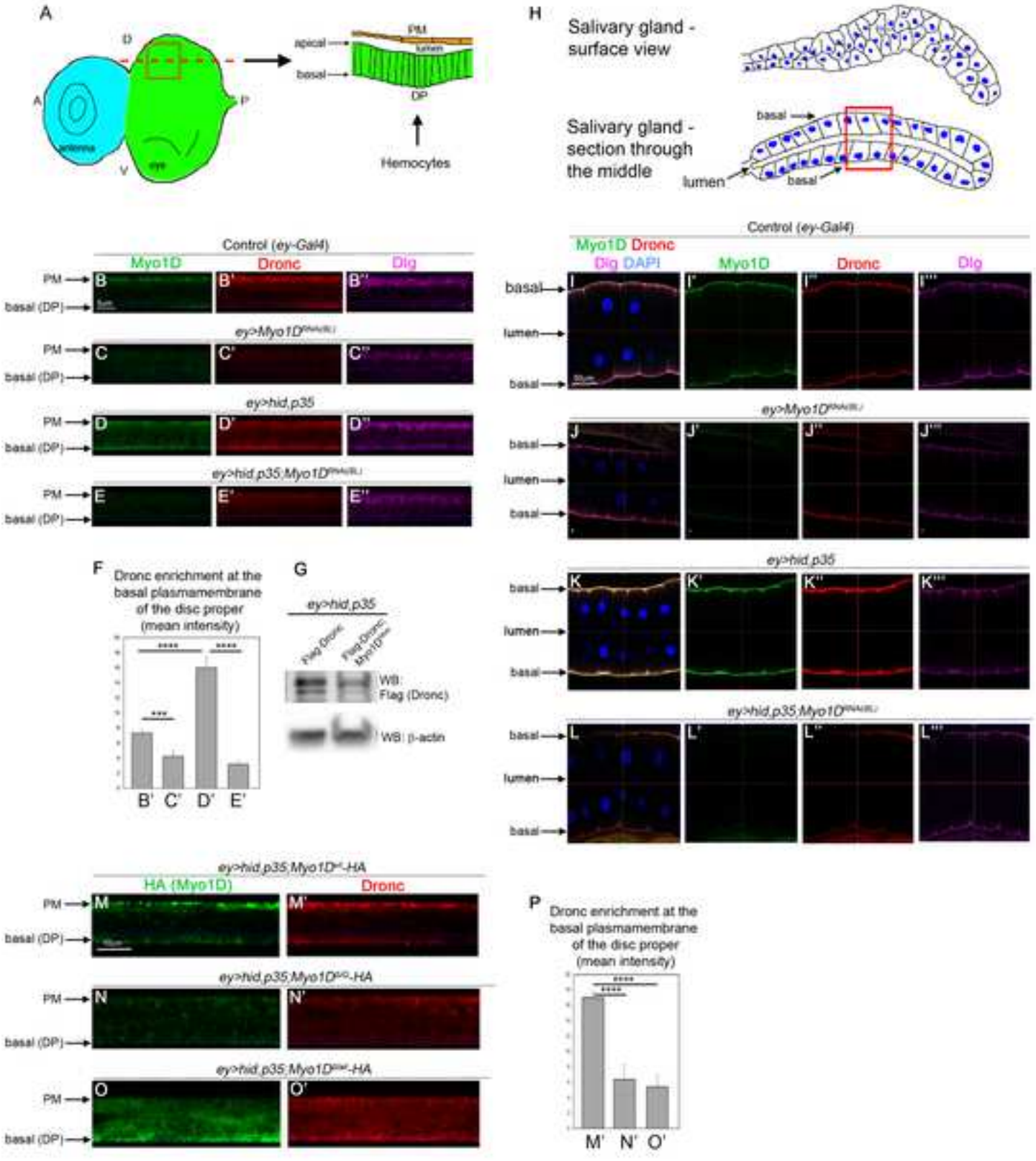

Figure 5

Click here to download Figure Figure 5.tif

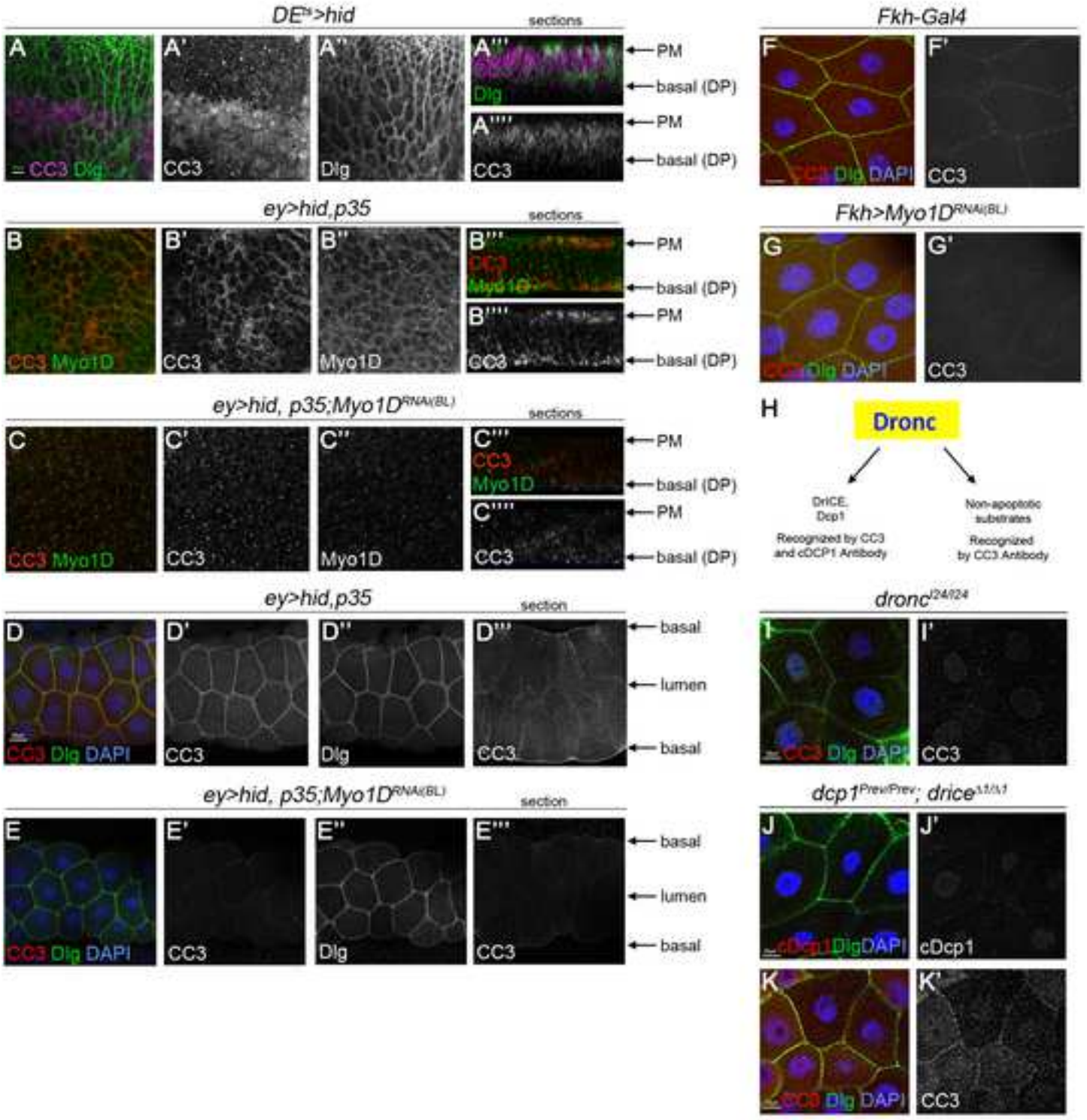

Figure 6

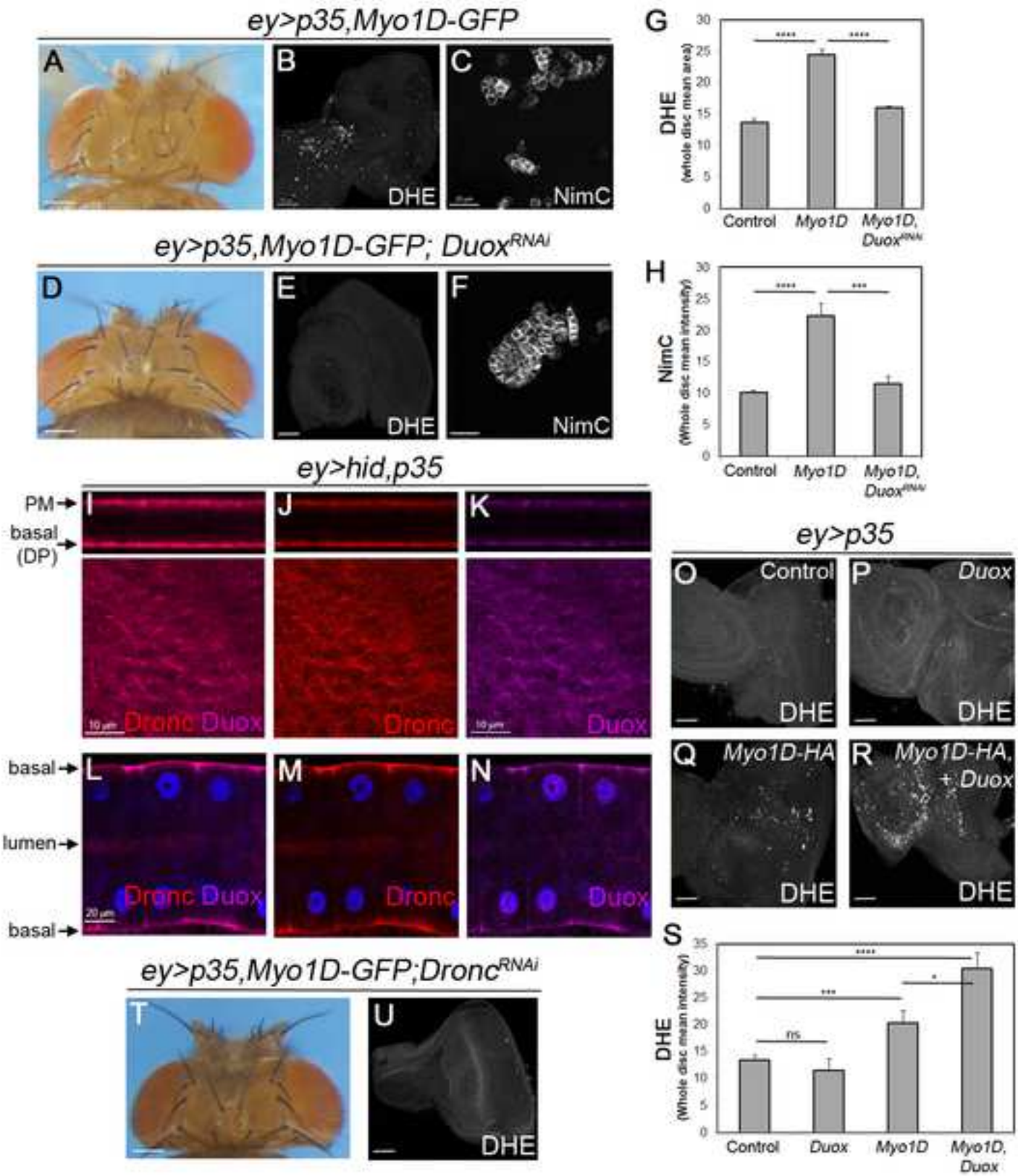

Figure 7

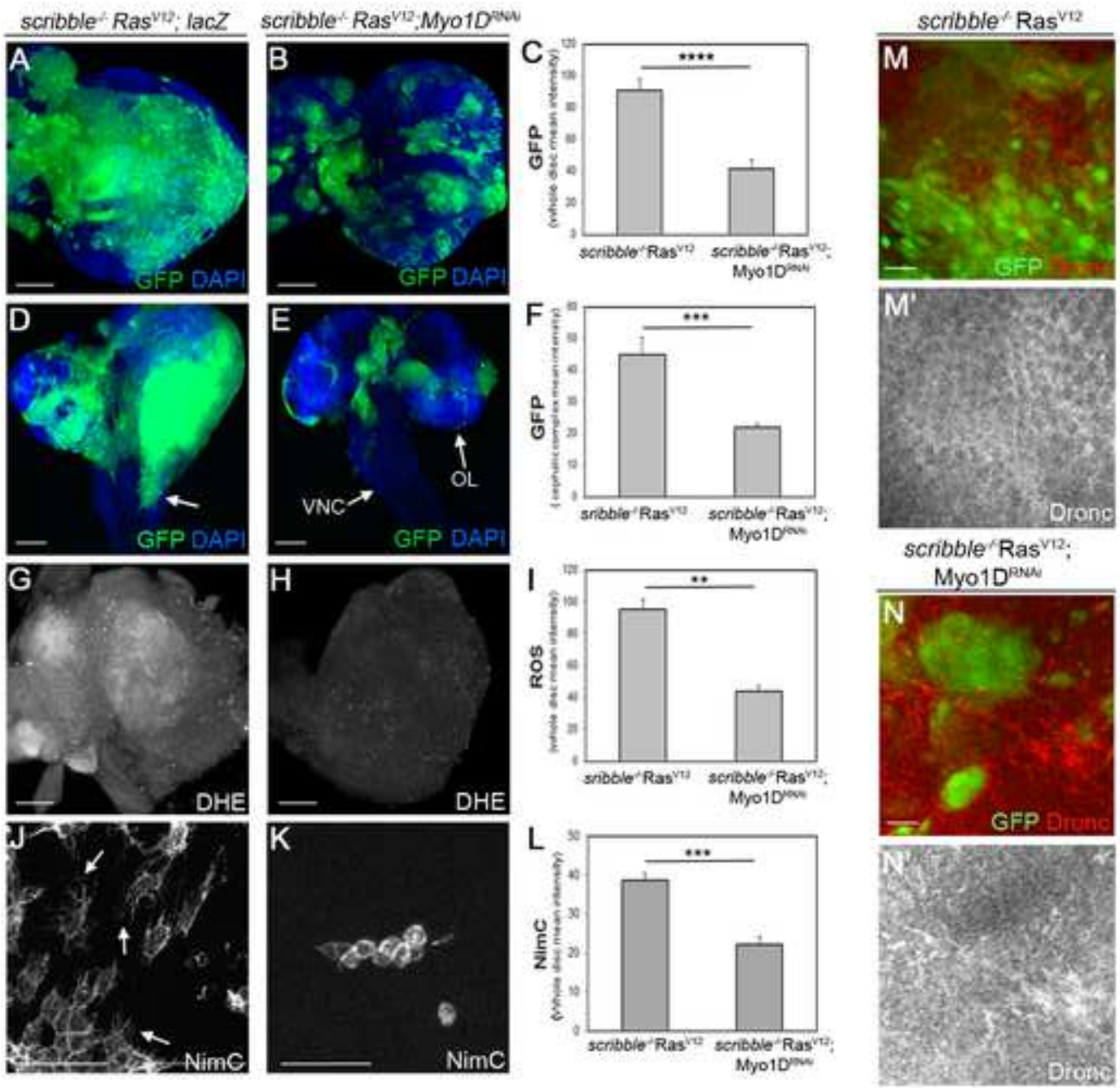

Figure 8

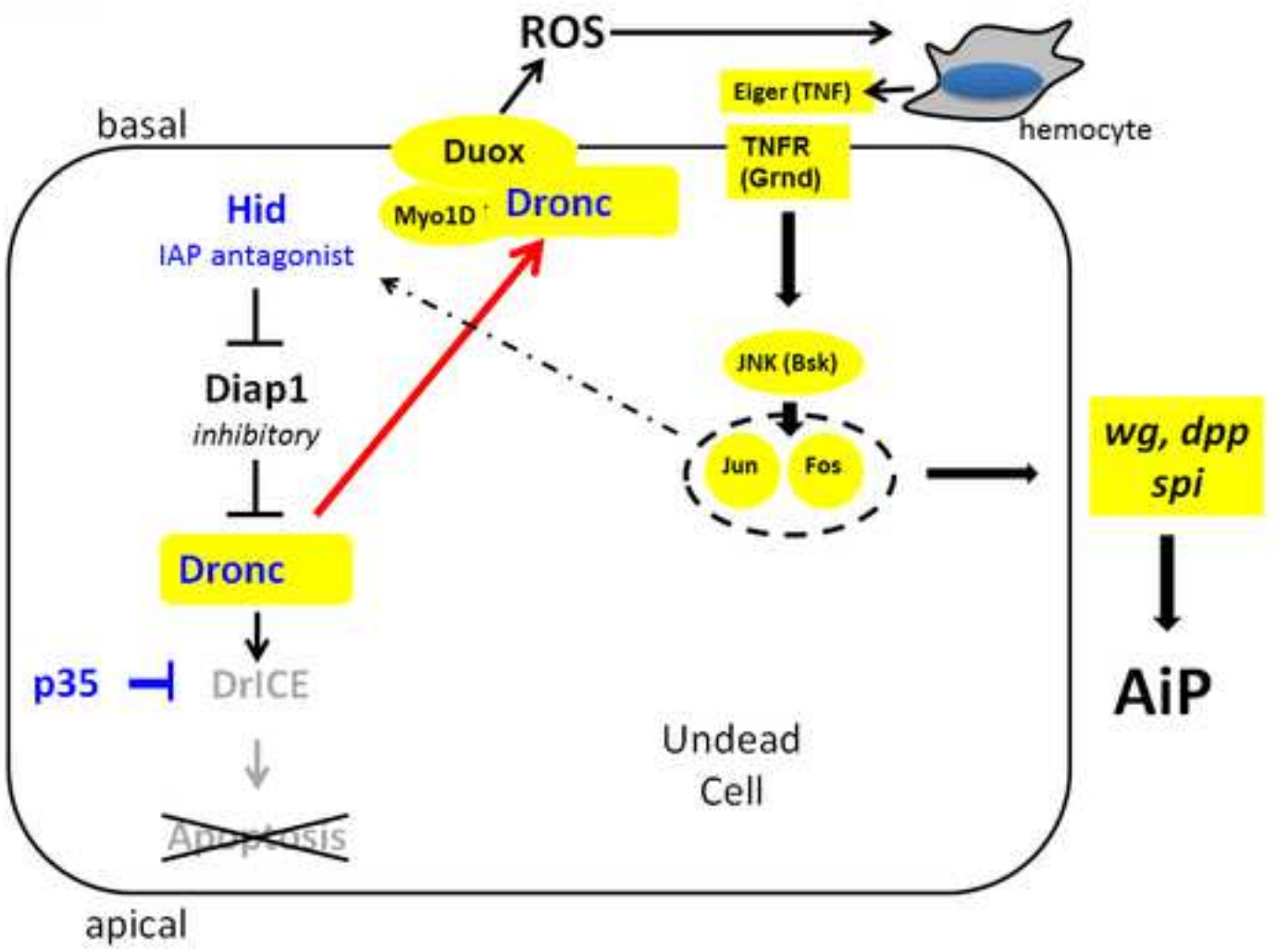

Supplemental figures and legends

Figure S1

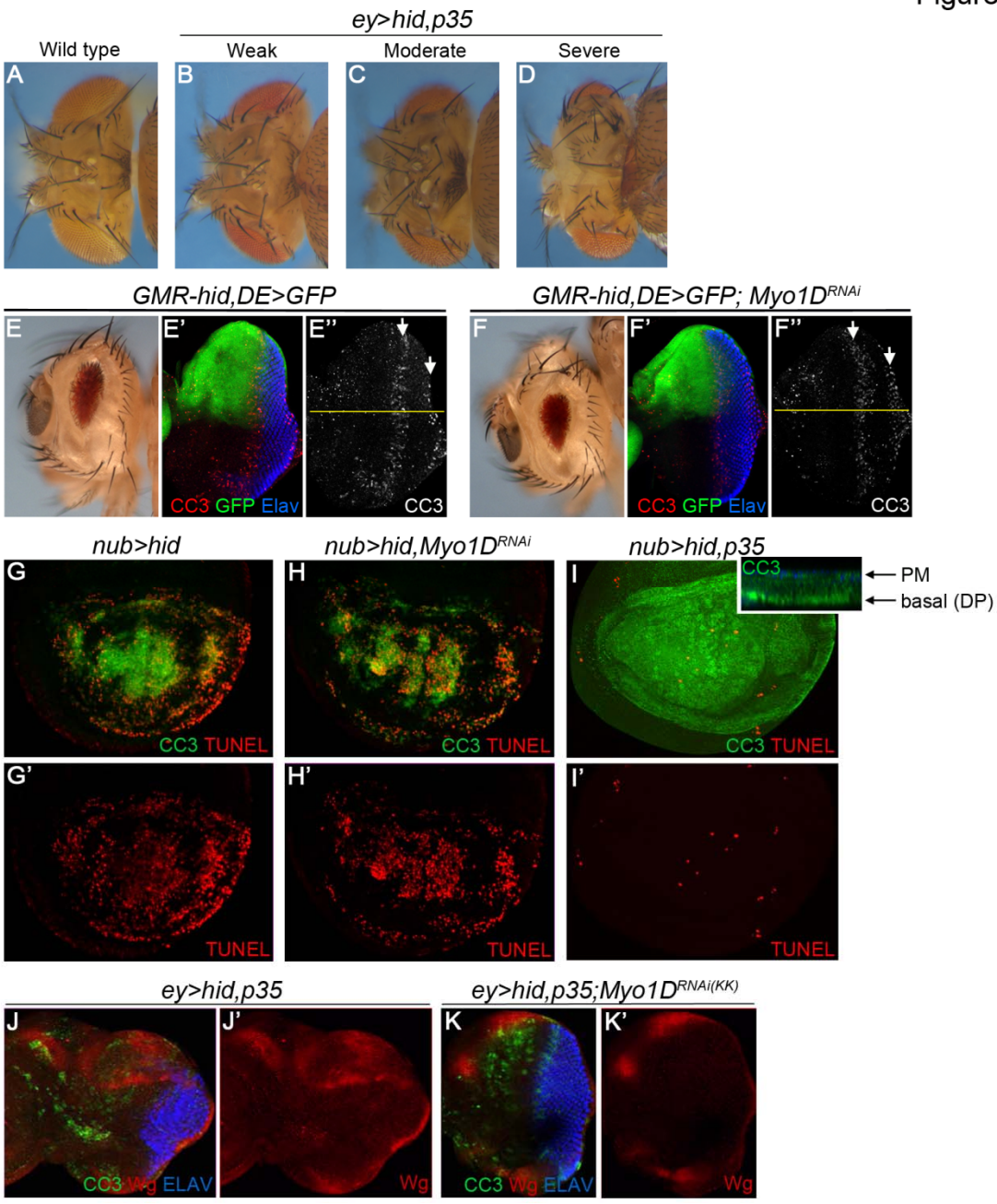

Figure S1. Information related to Figure 1.

(**A-D**) Representative examples of the phenotypic classes of *ey>hid,p35*-induced overgrowth of the head capsules. Overgrowth was scored based on qualitative screening criteria as (B) weak

(presence of additional bristles and ocelli), (C) moderate (expansion of head capsule width) or (D) severely overgrown (strong amorph head capsule overgrowth at the expense of eyes). (A) wild-type fly head.

(**E-F’’**) The eye ablation phenotype of *GMR-hid* (E) is caused by two apoptotic waves (arrows) in the eye imaginal disc (E’’; arrows; CC3-cleaved caspase3) (Fan and Bergmann, 2014). *Myo1D* RNAi in the dorsal half of the *GMR-hid* eye disc using *dorsal eye-* (*DE-*)*Gal4* does not modify the eye phenotype (F) nor the cell death pattern in the eye disc (F’’). The *DE-Gal4* driver is expressed dorsally as indicated by GFP expression (green) (E’,F’) and the yellow line in (E’’,F’’). Elav labels photoreceptor neurons (blue in E’,F’).

(**G-I’**) Cleaved caspase 3 (CC3, green) and TUNEL labeling (red) of apoptotic (*nub>hid*) wing imaginal discs of indicated genotype. While *p35* expression suppresses TUNEL-labeling of apoptosis (I,I’), *Myo1D* RNAi does not (H,H’).CC3 labeling persists in undead (*p35*-inhibited) *nub>hid* wing imaginal discs (I), but shifts towards the basal side of the plasmamembrane of disc proper (DP) cells (inset in I).

(**J-K’**) The strong Wg labeling (red) in *ey>hid,p35* eye discs (J,J’) is significantly reduced by *Myo1D* RNAi line KK102456 (K,K’).

Figure S2

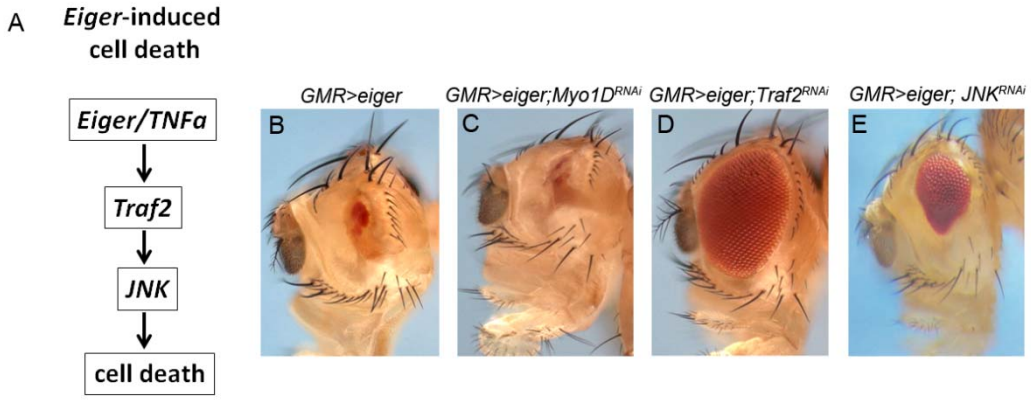

Figure S2. *Myo1D* is not acting in the Eiger signaling pathway. (Related to Figure 1)

Myo1D RNAi (KK102456) (C) is unable to suppress the strong eye ablation phenotype caused by *GMR-Eiger* (B) in contrast to *Traf2* RNAi (D) and JNK RNAi (E) which are known players in Eiger signaling (A).

Figure S3

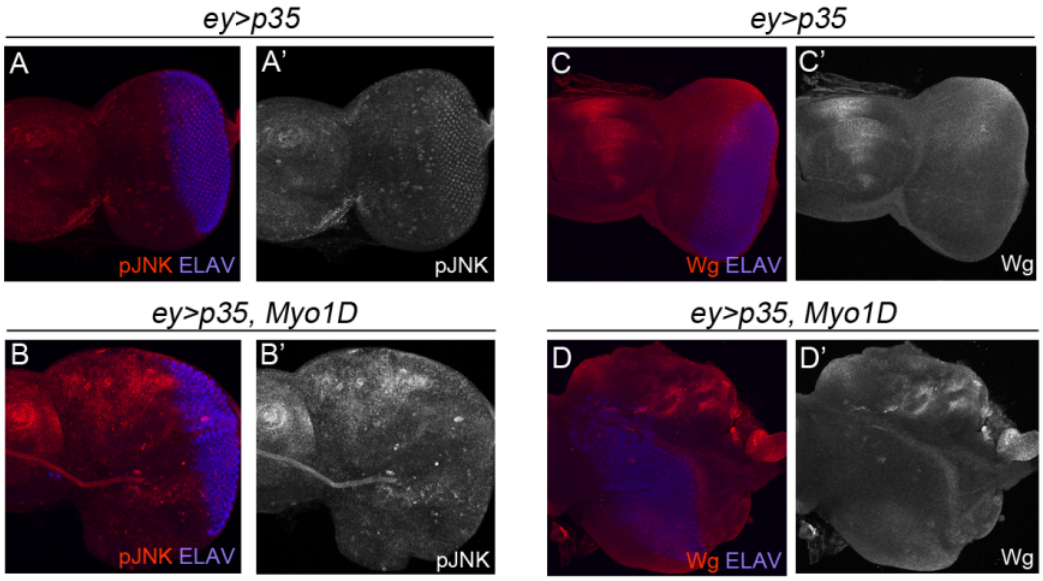

Figure S3. Misexpression of *Myo1D* in *ey>p35* eye imaginal discs induces JNK activity (pJNK) and increased Wg protein expression. (Related to Figure 1)

(**A-B'**) Misexpression of *Myo1D* in *ey>p35* eye/antennal imaginal discs induces strong JNK activity (pJNK) (B,B') and overgrown discs compared to *ey>p35* control discs (A,A').

(**C-D'**) Misexpression of *Myo1D* in *ey>p35* eye/antennal imaginal discs induces strong Wg expression (D,D') and overgrown discs compared to *ey>p35* control discs (C,C').

Figure S4

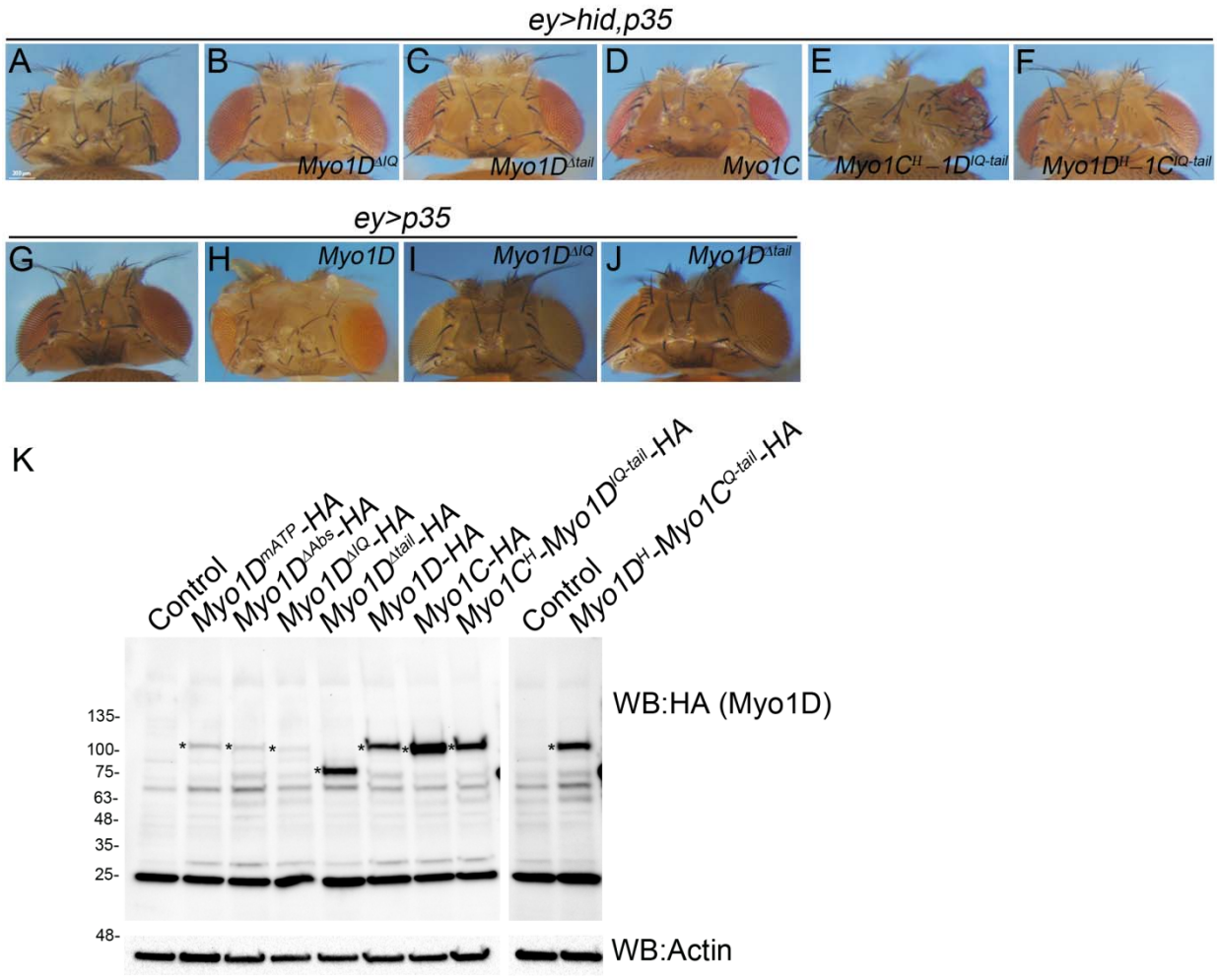

Figure S4. Specific requirement of neck (IQ) and tail domains for Myo1D's function in AiP. (Related to Figure 2)

(**A-F**) Head capsules of *ey>hid,p35* (A) flies expressing the indicated transgenes (B-F).

(**G-J**) Head capsules of *ey>p35* (G) flies expressing the indicated transgenes (H-J).

(**K**) Immunoblot analysis to examine expression levels of indicated wild-type and mutant *Myo1D-HA*, *Myo1C-HA* and chimeric transgenes in *ey>hid,p35* background. In each lane, extracts of four adult heads were loaded. The blot was probed with anti-HA antibody. A loading control blot was probed with anti-Actin antibody. Three independent immunoblot experiments gave comparable results.

Figure S5

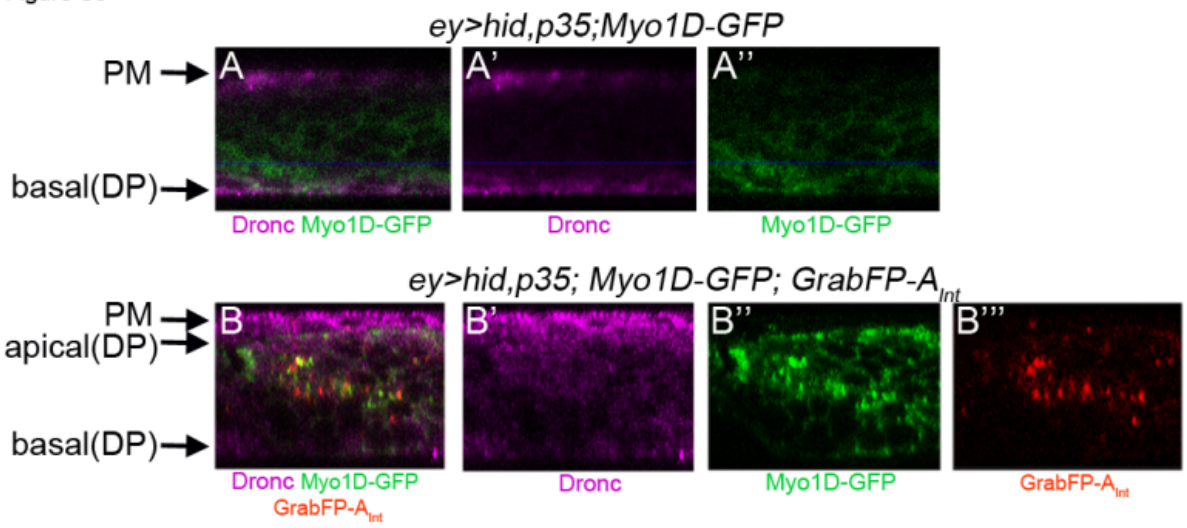

Figure S5. Mis-localization of Dronc by apical targeting of Myo1D-GFP with GrapFP-A$_{Int}$. (Related to Figure 4)

(**A-A''**) Sections of undead (*ey>hid,p35*) eye imaginal disc co-expressing *UAS-Myo1D-GFP* labeled for endogenous Dronc protein (magenta) and Myo1D-GFP (green). Dronc protein is localized at the peripodial membrane (PM) and the basal side of the plasmamembrane of the disc proper (DP) (arrows).

(**B-B'''**) Sections of undead (*ey>hid,p35*) eye imaginal disc co-expressing *UAS-Myo1D-GFP* and *UAS-GrabFP-A$_{Int}$* labeled for endogenous Dronc protein (magenta), Myo1D-GFP (green) and *GrabFP-A$_{Int}$* (red). *GrabFP-A$_{Int}$* encodes an apically-localized GFP-specific nanobody that targets GFP-containing fusion proteins to the apical side of the plasmamembrane (Harmansa et al., 2017). Although GrabFP-A$_{Int}$ protein does not perfectly localize to the apical side of the plasmamembrane (B'''), it disrupts the basal localization of Myo1D-GFP (B''). Consequently, the basal localization of Dronc is also abolished (B').

Figure S6

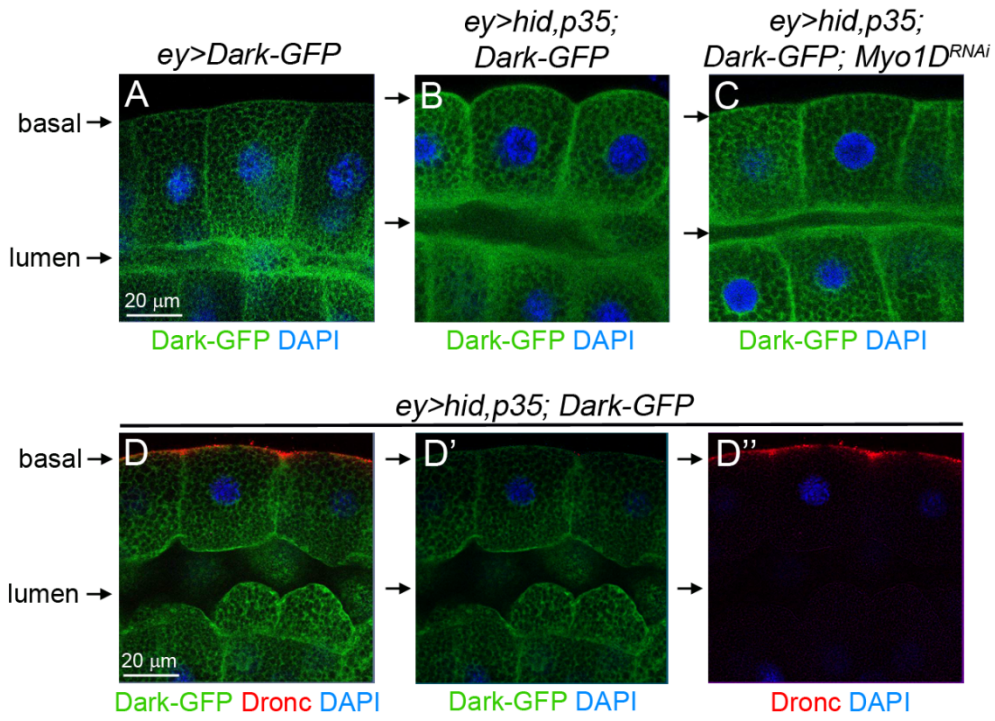

Figure S6. Subcellular localization of Dark-GFP is not changed in undead salivary gland (SG) cells and is not dependent on *Myo1D*. (Related to Figure 4)

Shown are confocal sections through the middle of SGs. Basal sides of SG cells and the lumen between them are indicated by arrows. DAPI (blue) labels nuclei.

(**A**) The subcellular localization of Dark-GFP (green) in control (*ey-Gal4*) SG cells. Scale bar: 20µm.

(**B**) The subcellular localization of Dark-GFP in undead (*ey>hid,p35*) SG cells is not significantly changed compared to (A).

(**C**) The subcellular localization of Dark-GFP in undead (*ey>hid,p35*) SG cells expressing *Myo1D* RNAi (BL33971) is not significantly changed compared to (B).

(**D-D''**) Comparison of the localization of endogenous Dronc (red) and mis-expressed Dark-GFP (green) proteins in undead larval SG cells. Dark-GFP labeling is cytosolic in SG cells, but also has a low level localization at the plasmamembrane, although it is very low at the basal side (D, D') where Dronc is localized (D''). Scale bar: 20 µm.